Microbial Pathogenesis 52 (2012) 285–291

Contents lists available at SciVerse ScienceDirect

Microbial Pathogenesis

journal homepage: www.elsevier.com/locate/micpath

Essential role of hormone-sensitive lipase (HSL) in the maintenance of lipid storage in *Mycobacterium leprae*-infected macrophages

Kazunari Tanigawa, Yang Degang, Akira Kawashima, Takeshi Akama, Aya Yoshihara, Yuko Ishido, Masahiko Makino, Norihisa Ishii, Koichi Suzuki*

Leprosy Research Center, National Institute of Infectious Diseases, 4-2-1 Aoba-cho, Higashimurayama, Tokyo 189-0002, Japan

ARTICLE INFO

Article history:
Received 18 April 2011
Received in revised form
9 February 2012
Accepted 14 February 2012
Available online 20 February 2012

Keywords:
Mycobacterium leprae
Leprosy
Hormone sensitive-lipase
Macrophage
Lipid droplet

ABSTRACT

Mycobacterium leprae (M. leprae), the causative agent of leprosy, parasitizes within the foamy or enlarged phagosome of macrophages where rich lipids accumulate. Although the mechanisms for lipid accumulation in the phagosome have been clarified, it is still unclear how such large amounts of lipids escape degradation. To further explore underlying mechanisms involved in lipid catabolism in *M. leprae*-infected host cells, we examined the expression of hormone-sensitive lipase (HSL), a key enzyme in fatty acid mobilization and lipolysis, in human macrophage THP-1 cells. We found that infection by live *M. leprae* significantly suppressed HSL expression levels. This suppression was not observed with dead *M. leprae* or latex beads. Macrophage activation by peptidoglycan (PGN), the ligand for toll-like receptor 2 (TLR2), increased HSL expression; however, live *M. leprae* suppressed this increase. HSL expression was abolished in the slit-skin smear specimens from patients with lepromatous and borderline leprosy. In addition, the recovery of HSL expression was observed in patients who experienced a lepra reaction, which is a cell-mediated, delayed-type hypersensitivity immune response, or in patients who were successfully treated with multi-drug therapy. These results suggest that *M. leprae* suppresses lipid degradation through inhibition of HSL expression, and that the monitoring of HSL mRNA levels in slit-skin smear specimens may be a useful indicator of patient prognosis.

1. Introduction

Leprosy is a chronic infectious disease caused by *Mycobacterium leprae* (*M. leprae*). Although its prevalence has declined over the last several decades due to the introduction of multi-drug therapy (MDT), leprosy still remains a major public health problem in many developing countries. In 2009, 244,796 new cases were registered worldwide [1]. *M. leprae* is a typical intracellular pathogen that parasitizes tissue macrophages (histiocytes) and Schwann cells of the peripheral nerves of the dermis. In 1966 Ridley and Jopling used clinical, histological and immunological criteria to classify leprosy patients across the spectrum, and suggested five member groups: Tuberculoid (TT), Borderline Tuberculoid (BT), Borderline (BB), Borderline Lepromatous (BL) and Lepromatous (LL) [2]. Lepromatous leprosy is a stable condition (patient status does not shift from these polar positions), while borderline lepromatous leprosy is immunologically unstable. Lepromatous leprosy is characterized by widespread skin lesions that form due to an impaired cellular immune response. The lesions consist of numerous bacilli that live in the foamy or enlarged lipid-filled phagosome within macrophages. Although lipid-laden macrophages are observed in other mycobacterial infections, including tuberculosis [3,4], the amount of lipid and the number of infected macrophages are most prominent in cases of lepromatous leprosy.

The PAT protein family is named after perilipin, adipophilin/adipose differentiation-related protein (ADRP) and the tail-interacting protein of 47 kDa (TIP47). Members of the PAT family are responsible for lipid transportation and lipid droplet formation in a variety of tissues and cultured cell lines, including adipocytes [5–8]. We previously reported that ADRP and perilipin play important roles in lipid accumulation in *M. leprae*-infected macrophages [9]. ADRP and perilipin localized to the phagosomal membrane of histiocytes, which contained numerous *M. leprae*, in the skin lesions of patients with lepromatous leprosy. *M. leprae* infection increased mRNA and protein expression of ADRP and perilipin in cultured human THP-1 monocytes. The results suggested that ADRP and perilipin contribute to the creation of

* Corresponding author. Laboratory of Molecular Diagnostics, Department of Mycobacteriology, Leprosy Research Center, National Institute of Infectious Diseases, 4-2-1 Aoba-cho, Higashimurayama, Tokyo 189-0002, Japan. Tel.: +81 42 391 8211; fax: +81 42 394 9092.
E-mail address: koichis@nih.go.jp (K. Suzuki).

0882-4010/$ – see front matter © 2012 Elsevier Ltd. All rights reserved.
doi:10.1016/j.micpath.2012.02.003

a lipid-rich environment that is favorable for *M. leprae* parasitization and survival in the host.

However, accumulated lipids are supposed to undergo degradation and reutilization by cells over time. In fact, fatty acids mobilized from stored triacylglycerols (TAG) are a major energy source in humans. Mobilization occurs through the consecutive action of three lipases: adipose triglyceride lipase (ATGL), monoacylglycerol lipase (MGL) and hormone-sensitive lipase (HSL) [10]. Among these, HSL was the first enzyme identified in the induction of lipo-catabolic action initiated by hormones and is the predominant lipase effector of catecholamine-stimulated lipolysis in adipocytes [11]. Therefore, ADRP/perilipin and HSL have opposing functions, *i.e.* lipid accumulation vs. its degradation. In addition to adipocytes, HSL is expressed in the cytoplasm of macrophages, pancreatic β cells, skeletal muscle cells, steroid producing cells, the intestine, and spleen [10]. HSL serine residues are phosphorylated by enzymes such as protein kinase A (PKA), 5′ AMP-activated protein kinase (AMPK) and mitogen-activated protein kinase (MAPK) to regulate the process of hormone-induced lipolysis [11].

To date, the molecular mechanism(s) that allows the phagosome of *M. leprae*-infected macrophages to escape lipolytic activities is not known. In this study, we investigate the expression and phosphorylation of HSL in *M. leprae*-infected cultured macrophages. We also examine clinical samples from leprosy patients and explore the impact of *M. leprae* on lipid metabolism in infected host cells.

2. Materials and methods

2.1. M. leprae isolation and cell culture

Hypertensive nude rats (SHR/NCrj-*rnu*), in which the Thai53 strain of *M. leprae* was actively grown [12,13], were kindly provided by Dr. Y. Yogi of the Leprosy Research Center, National Institute of Infectious Diseases, Japan. *M. leprae* was isolated as previously described [14,15]. The human premonocytic cell line THP-1 was obtained from the American Type Culture Collection (ATCC; Manassas, VA). The cells were cultured in 10 cm tissue culture dishes in RPMI medium supplemented with 10% charcoal-treated fetal bovine serum (FBS), 2% non-essential amino acids and 50 mg/ml penicillin/streptomycin at 37 °C in 5% CO_2 [9,16]. Typically, 3×10^7 bacilli were added to 3×10^6 THP-1 cells, for a multiplicity of infection (MOI) of 10. Peptidoglycan (PGN) and lipopolysaccharide (LPS) were purchased from Sigma (St Louis, MO) and added at final concentrations of 2 μg/ml and 1 μg/ml, respectively. TLR2 antibody (sc-21759; Santa Cruz Biotechnology, Santa Cruz, CA) was used at a final concentration of 5 μg/ml.

2.2. Immunohistochemistry and lipid staining

THP-1 cells were grown on glass coverslips in 24-well plates for 24 h before the culture medium was exchanged with RPMI 1640 containing *M. leprae*. Control and *M. leprae*-infected THP-1 cells were fixed in 10% paraformaldehyde for 10 min. They were then washed with Dulbecco's phosphate buffered saline (DPBS) containing 0.4% Triton-X 100 (DPBST), incubated with anti-HSL antibody (Cell Signaling Technology, Danvers, MA) diluted to 1:100 for 24 h at 4 °C and washed again with DPBST. The signal was detected using peroxidase-labeled streptavidin-biotin (LSAB2 Kit; DAKO, Carpinteria, CA) and 3,3-diaminobenzidine tetrahydrochloride (DAB) [9]. Cells were counterstained with methylene blue. Lipid staining was performed with oil red O (Muto Pure Chemicals, Tokyo, Japan) for 10 min, and counterstained with hematoxylin for another 5 min.

2.3. RNA preparation and RT-PCR

RNA from cultured cells was prepared using RNeasy Mini Kits (Qiagen Inc., Valencia, CA) as described previously [9,16]. RNA preparation from slit-skin smear samples was performed as described [9]. Briefly, stainless steel blades (Feather Safety Razor Co., LTD, Osaka, Japan) used to obtain slit-skin smear specimens were rinsed in 1 ml of sterile 70% ethanol, then the tube was and centrifuged at 20,000 × g for 1 min at 4 °C. After removing the supernatant, RNA was purified with the same protocol used for cultured cells. RNA was eluted in 20 μl of elution buffer and treated with 0.1 U/μl of DNase I (TaKaRa Bio, Kyoto, Japan) at 37 °C for 60 min in order to degrade any contaminating genomic DNA. RNA concentration and purity were assessed using a NanoVue spectrophotometer (GE Healthcare, Little Chalfont, UK). Total RNA from each sample was reverse-transcribed to cDNA using a High Capacity cDNA Reverse Transcription Kit (Applied Biosystems, Foster City, CA) [9]. The following primers were used to amplify specific cDNAs: HSL: 5′-CTCCTCATGGCTCAACTCCTTCC-3′ (forward) and 5′-AGGGGTTCTTGACTATGGGTG-3′ (reverse); ADRP: 5′-TGTGGAGAAGACCAAGTCTGTG-3′ (forward) and 5′-GCTTCTGAACCAGATCAAATCC-3′ (reverse); and actin: 5′-AGCCATGTACGTAGCCATCC-3′ (forward) and 5′-TGTGGTGGTGAAGCTGTAGC-3′ (reverse). Touchdown PCR was performed using a PCR thermal cycler DICE (TaKaRa Bio) as previously described [9]. The products were analyzed by 2% agarose gel electrophoresis.

Slit-skin smear samples from leprosy patients were used according to the guidelines approved by the National Institute of Infectious Diseases, Tokyo, Japan.

2.4. Protein preparation and Western blot analysis

Cellular protein was extracted and analyzed as previously described [9,17]. Briefly, cells were lysed in a lysis buffer containing 50 mM HEPES, 150 mM NaCl, 5 mM EDTA, 0.1% NP40, 20% glycerol, and protease inhibitor cocktail (Complete Mini, Roche, Indianapolis, IN) for 1 h. After centrifugation, the supernatant was transferred and 10 μg of protein was used for analysis. Samples were heated in SDS sample loading buffer at 95 °C for 5 min and loaded on a polyacrylamide gel. After electrophoresis, proteins were transferred to a PVDF membrane using a semi-dry blotting apparatus (Bio-Rad, Hercules, CA). The membrane was washed with PBST (PBS with 0.1% Tween 20), blocked in blocking buffer (PBST containing 5% nonfat milk) overnight, and then incubated with either anti-HSL, anti-phospho-HSL (Ser^{563}) or anti-phospho-HSL (Ser^{565}) antibody (Cell Signaling Technology, 1:2000 dilution). After washing with PBST, the membrane was incubated for 1 h with biotinylated donkey anti-rabbit antibody (GE Healthcare, 1:2000 dilution) and streptavidin-HRP (GE Healthcare, 1:10,000 dilution) according to the manufacturer's protocol. The signal was developed using ECL Plus Reagent (GE Healthcare).

3. Results

3.1. HSL expression is suppressed in macrophages infected with M. leprae

To confirm the possible relationship between lipid accumulation and HSL expression in macrophage, we infected *M. leprae* in THP-1 cells and performed oil red O staining and HSL and ADRP immunostaining. Lipid droplets were not evident in control THP-1 cells (Fig. 1A), but accumulation was clearly demonstrated in cells 24 h after *M. leprae* infection (Fig. 1B). ADRP expression, which contributes to lipid intake, was not evident in control cells, but was significantly increased following *M. leprae* infection as previously reported (Fig. 1C and D, respectively) [9]. Conversely, HSL expression

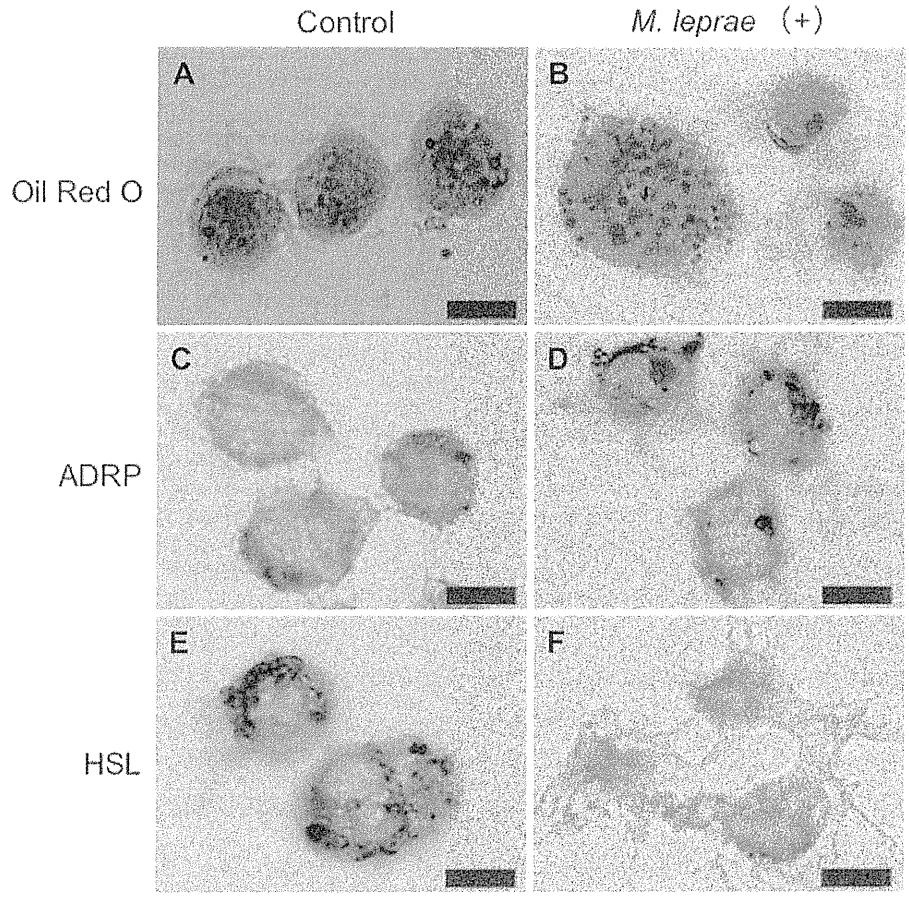

Fig. 1. HSL expression in macrophages is reduced by *M. leprae* infection. THP-1 cells grown on glass coverslips in 24-well plates for 24 h were used as a control or were infected with *M. leprae* for 24 h, then subjected to oil red O staining (A and B), ADRP immunostaining (C and D) or HSL immunostaining (E and F). Bars = 10 μm.

was clearly visible in the control THP-1 cells before infection, but it was significantly reduced by 24 h after *M. leprae* infection (Fig. 1E and F). Overall, oil red O staining was detected in 14.8% (9/61) of control THP-1 cells, whereas the percentage of *M. leprae*-infected cells increased to 91.7% (89/97). Similarly, only 16.9% (12/71) of cells were weakly immunostained with ADRP, but 88.2% (90/102) were strongly stained following infection. HSL-positive cells were observed in 80.3% (53/66) of control cells, but in only 7.2% (6/83) following *M. leprae* infection. These results suggested that the lipolytic pathway is constitutively activated in the control THP-1 cells, as evidenced by strong HSL staining; however, it was significantly suppressed by *M. leprae* infection, which in turn would reduce lipolysis in infected cells and maintain cellular lipids.

3.2. Only live *M. leprae* suppresses HSL expression

We next evaluated changes in HSL mRNA and protein levels in THP-1 cells following *M. leprae* infection. Reverse transcription polymerase chain reaction (RT-PCR) analysis revealed that HSL mRNA levels were significantly decreased 6 h after *M. leprae* infection (Fig. 2A, left panel). HSL protein levels, as assessed by Western blot analysis, were also decreased by 6 h after infection (Fig. 2B, left panel). In both cases ADRP levels were increased as previously shown [9].

In order to clarify whether the observed decrease of HSL was specific to viable *M. leprae* or non-specific to phagocytosis, we compared the effects of live *M. leprae* with dead (heat-killed) *M. leprae* or latex beads on HSL expression. The mRNA and protein levels of HSL were transiently decreased at 6 h following exposure to dead *M. leprae* and latex beads, but they had mostly recovered to the original levels by 48 h (Fig. 2A and B, middle and right panels). In contrast, ADRP levels were transiently increased by dead *M. leprae* or latex beads at 6 h, but had returned to the original levels in 48 h. The transient effects of dead bacilli and the sustained effects of live bacilli on HSL suppression are similar to the effects of dead and live bacilli on the phagosomal localization of CORO1A [16,18]. Together, these results suggest that the phagocytosis of certain particles will transiently, but not permanently, decrease HSL expression; however, only live *M. leprae* was capable of maintaining the suppression of HSL expression (Fig. 2A and B).

Phosphorylation of HSL on Ser^{563} by PKA and Ser^{565} by 5′-AMP-activated protein kinase (AMPK) is required for the translocation and the functional activity of HSL [19,20]. Therefore, these serine residues were evaluated to determine if they are dephosphorylated following *M. leprae* infection. Western blot analysis using phosphorylation-specific antibodies revealed a rapid decrease in phosphorylation of HSL at both Ser^{563} and Ser^{565} 1 h after *M. leprae* infection (Fig. 2C). This result further confirmed that *M. leprae* infection not only reduces HSL expression, but potentially abrogates its function as well.

3.3. Innate immune activation increases HSL expression, but *M. leprae* infection reverses

The induction of innate immunity by activation of toll-like receptors (TLRs) modulates the expression of host proteins and

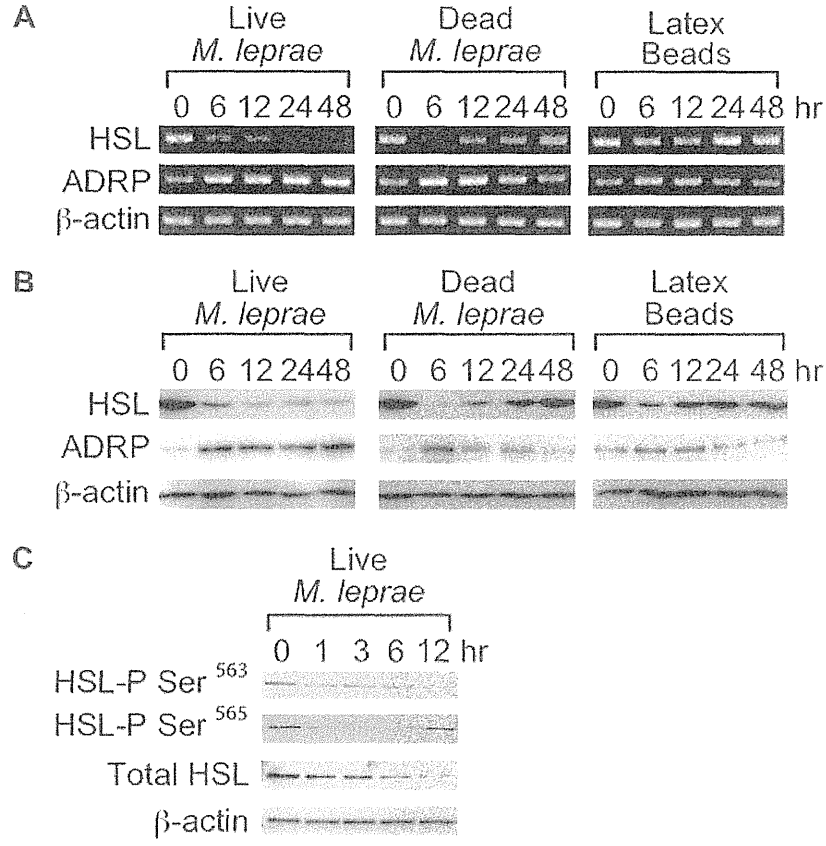

Fig. 2. Only live *M. leprae* persistently reduces HSL mRNA and protein levels in infected cells. THP-1 cells were cultured in a six-well plate and infected with live *M. leprae*, heat killed (80 °C for 30 min) *M. leprae* or latex beads. After incubating for the indicated period of time, total RNA and total cellular protein were purified and RT-PCR analysis (A) and Western blot analysis (B) for HSL, ADRP and β-actin were performed. Phosphorylation of HSL on Ser^{563} and Ser^{565} was evaluated by Western blot analysis in *M. leprae*-infected cells using specific antibodies (C).

contributes to host defense against *M. leprae* [9,16,17,21]. Therefore, the possible effect of PGN, a ligand for TLR2, on HSL expression levels was examined. When PGN was added to the culture medium of THP-1 cells, HSL mRNA expression was increased at 6 h and high levels of expression were maintained up to 24 h (Fig. 3A). HSL protein levels were also increased and high levels were still evident even 48 h after treatment (Fig. 3B). Since infection of live *M. leprae* significantly suppressed HSL expression (Fig. 2), we evaluated the possible effect of *M. leprae* infection on the effect of PGN. When *M. leprae* was added with PGN, the increase of PGN-induced HSL mRNA and protein levels observed at 6 h was abolished (Fig. 3C and D vs. Fig. 3A and B, respectively). Instead, HSL mRNA and protein levels had decreased by 48 h (Fig. 3C and D).

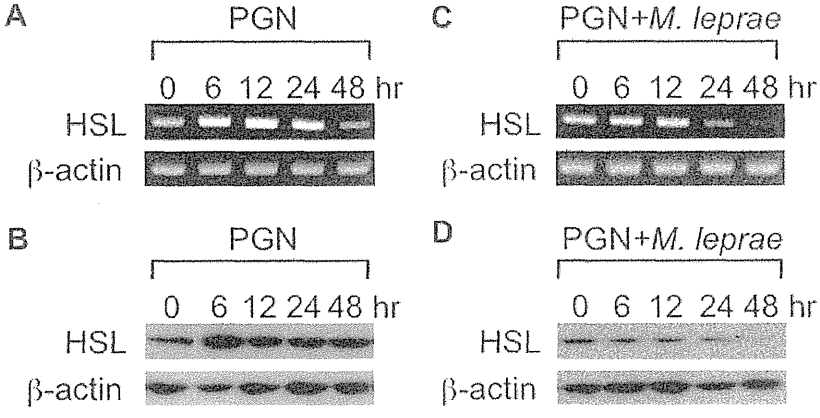

Fig. 3. *M. leprae* inhibits the ability of PGN to induce the expression of HSL. THP-1 cells were cultured in a six-well plate and treated with PGN (A and B), PGN plus *M. leprae* (C and D). After incubating for the indicated time, total RNA and total cellular protein for each experiment were purified and RT-PCR analysis (A and C) and Western blot analysis (B and D) for HSL and β-actin were performed.

TLR2 neutralizing antibody was able to suppress the PGN-mediated induction of HSL mRNA and protein levels (Fig. 4C vs. A and D vs. B, respectively), suggesting that the action of PGN is mediated through TLR2. Although activation of TLR4 by LPS enhanced HSL expression, *M. leprae* infection abolished LPS-induced HSL mRNA and protein levels (Fig. 4G vs. E and H vs. F, respectively). These results suggest that lipolysis is activated by TLR activation. However, infection of live *M. leprae* inhibits the TLR-mediated increase of HSL expression despite the fact that PGN is actually a component of the *M. leprae* cell wall. Therefore, *M. leprae* could potentially activate a hitherto unrecognized TLR-independent pathway that results in inhibition of TLR-mediated HSL activation in order to prevent the degradation of lipids in infected phagosomes.

3.4. Appearance of HSL mRNA in slit-skin smears correlates with clinical course of leprosy

All of the *in vitro* studies described herein indicated that *M. leprae* infection decreases HSL expression, which may correlate with the maintenance of a lipid-rich environment within the phagosome. To examine HSL expression in the skin lesions of leprosy patients, HSL mRNA levels were evaluated in slit-skin smear specimens by RT-PCR analysis. HSL mRNA was not detected in the five lepromatous leprosy (LL) patients nor in four out of seven borderline lepromatous leprosy (BL) patients, but was clearly detected in two of these patients (Fig. 5A, cases 8 and 12). Interestingly, these two cases, whose HSL mRNA levels were clearly detectable, exhibited a 'type 1 lepra reaction (or upgrading reaction)' after treatment (at one year for case 8 and three months for case 12), which is thought to be a cell-mediated, delayed-type of hypersensitivity immune response.

We also analyzed slit-skin smear samples from four patients who received MDT treatment, which consisted of diaphenylsulfone, clofazimine and rifampicin, as per WHO protocol. While HSL mRNA was not detected before treatment, HSL expression was induced (or recovered) after MDT treatment in all four cases (Fig. 5B). These results indicate that HSL expression is significantly suppressed following *M. leprae* infection in LL and BL patients; however, it reappeared in untreated patients who might have a potentially active immune response to *M. leprae* and in those whose bactericidal activity is enhanced by effective treatment.

4. Discussion

In this report, we first demonstrated that *M. leprae* suppresses the expression of HSL mRNA and protein in infected macrophages. Only live *M. leprae* could sustain suppressed levels of HSL, although phagocytosis itself only transiently decreased HSL levels. This situation is quite similar to the induction of lipid droplet-associated proteins, ADRP and perilipin, in macrophages infected with *M. leprae* as previously reported [9]. In that study, only live *M. leprae* infection could induce and maintain high expression levels of ADRP and perilipin. The present study provides another mechanism by

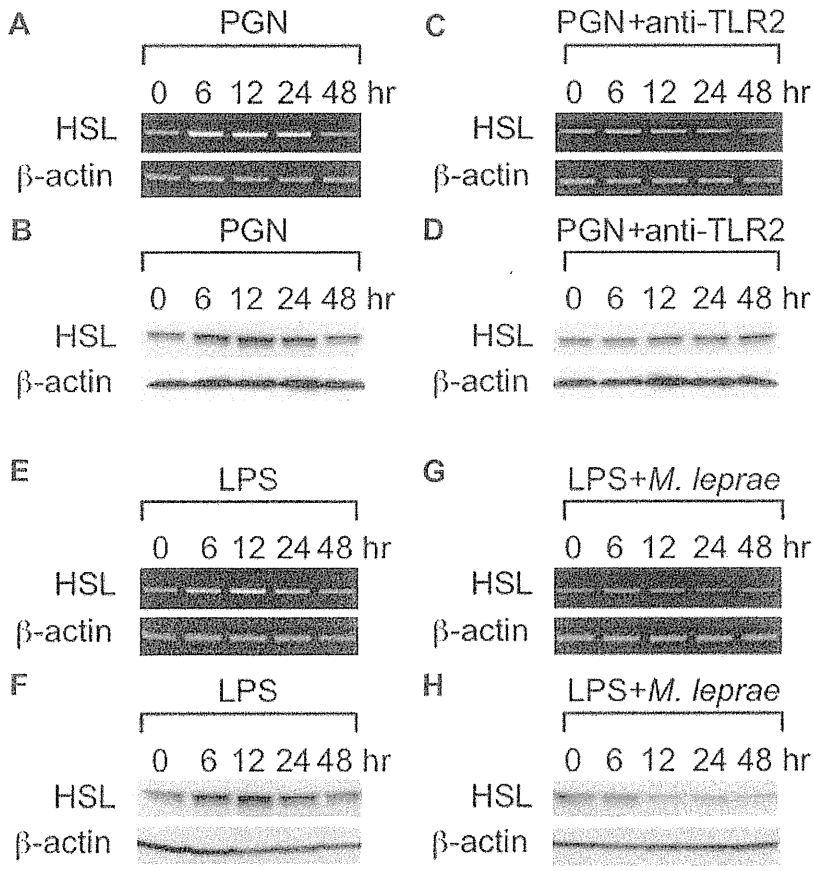

Fig. 4. TLR-mediated increase of HSL expression and its suppression by *M. leprae* infection. THP-1 cells were cultured in a six-well plate and treated with PGN (A and B), PGN plus TLR2 neutralizing antibody (C and D) or LPS (E and F) or LPS plus *M. leprae* (G and H). After incubating for the indicated time, mRNA expression or protein levels of HSL were evaluated by RT-PCR analysis (A, C, E and G) and Western blot analysis (B, D, F and H).

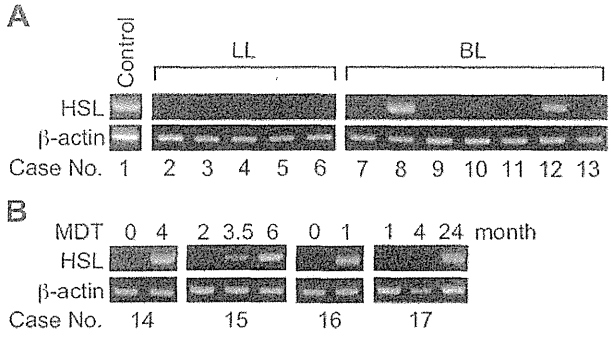

Fig. 5. Detection of HSL mRNA in slit-skin smear samples from leprosy patients. RNA was isolated from slit-skin smear specimens taken from five LL patients and seven BL patients for RT-PCR analysis (A). Cases 8 and 12 developed type 1 lepra reactions after MDT treatment. RNA isolated from four BL patients before and after MDT for the indicated period of time, was also used for RT-PCR analysis (B). The control sample was obtained from patients with skin granulomas where *M. leprae* was not found.

which *M. leprae* maintains host cell lipids, namely by suppressing their degradation.

Activation of the TLR signaling pathway by PGN increased HSL expression, indicating that activation of the innate immune response may induce lipid degradation that makes it difficult for *M. leprae* to survive within infected phagosomes. *M. leprae* infection not only suppressed HSL expression, but also inhibited the ability of PGN to increase HSL expression. We previously showed that PGN suppresses expression of ADRP and perilipin, and also significantly reduces expression of CORO1A, also known as tryptophan aspartate-containing coat protein (TACO), which contributes to the inhibition of lysosomal fusion and accounts for the survival of bacilli [9,16,17]. *M. leprae* infection invalidates all of these effects of PGN and thus maintains levels of CORO1A, ADRP and perilipin, and reduces HSL expression, thus ensuring a favorable phagosome environment for itself. These results showing that *M. leprae* and PGN, a cell wall component of *M. leprae*, have quite different effects are somewhat contradictory. It is plausible to speculate that some *M. leprae* components can activate a pathway that counteracts TLR signaling.

Suppression of HSL, in addition to the induction and phagosomal translocation of ADRP/perilipin and CORO1A, would reduce degradation of stored lipids, thereby maintaining the lipid-rich environment in the parasitized phagosome where *M. leprae* lives. *M. leprae* possesses only a small number of functional genes, which likely makes it difficult for the bacilli to survive without relying on host cell metabolism [14–16,22]. Therefore, *M. leprae* may regulate the expression of host genes that accumulate and maintain cellular lipids in order to utilize them as an essential nutrient for survival. Recent studies suggest that *Mycobacterium tuberculosis (M. tuberculosis)* persists within lipid-rich foamy phagosomes, while its translocation into the cytosol may relate to caseation and virulence [23–27]. Therefore, intracellular lifestyle and lipid requirements might differ substantially between *M. tuberculosis* and *M. leprae*, partly reflecting the massive gene decay in *M. leprae* [22]. Whether the small lipid droplets seen in *M. leprae*-infected cells (Fig. 1B) fuse with phagosomes containing *M. leprae* is still to be determined.

There was once debate over whether the lipids originate from *M. leprae* cell wall components or from the host [28,29]. It was suggested that lipids and fatty acids were important carbon sources for *M. leprae* in infected macrophages where the oxygen tension gradient is low [30]. It is now known that mycobacteria induce the accumulation of 1-palmitoyl-2-(5,6-epoxyisoprostane E2)-sn-glycero-3-phosphorylcholine (PEIPC), a host-derived oxidized phospholipid, and is similar to the formation of foamy cells found in atherosclerotic lesions [31,32]. Of interest, *M. tuberculosis* has a large number of proteins involved in lipid metabolism, including at least one HSL family protein. However, *M. leprae* seems to have a small number of such genes, and no HSL-like genes were identified (http://genolist.pasteur.fr/Leproma/).

The lipid degradation process in adipocytes involves both HSL and perilipin [33]. Both are polyphosphorylated by protein kinase A (PKA), and phosphorylation of perilipin is required for the translocation of HSL from the cytosol to the surface of the lipid droplet, which is a critical step in the lipolytic reaction [34]. Furthermore, there is growing evidence that both perilipin and comparative gene identification-58 (CGI-58) protein act as scaffold proteins on lipid droplets in adipocytes [35]. We demonstrated that live *M. leprae* not only suppresses HSL protein expression, but that it also phosphorylates two serine residues, Ser^{563} and Ser^{565}, which are essential for its action. HSL expression is modulated by energy level changes in a variety of situations, such as obesity [36], type 2 diabetes mellitus [37] and in cultured adipocytes [38,39]. However, there have been no reports that pathogenic microorganisms have the ability to modulate HSL expression. Since *M. tuberculosis* and *Mycobacterium avium* utilize host lipids [40,41], our finding may highlight an important mechanism by which these bacteria interact and modify host gene expression. Phosphorylation of HSL occurs at multiple sites, including Ser^{563}, which is believed to be mutually exclusive with phosphorylation of HSL at the non-PKA site Ser^{565} [19,20]. Therefore, the observed decrease of HSL phosphorylation might be due to down-regulation of PKA or induction of a non-functional kinase following infection with *M. leprae*.

HSL expression was not detected in slit-skin smear samples from any of the LL patients and most of the BL patients examined in this study. Two BL patients who showed detectable levels of HSL mRNA developed a type 1 lepra (or reversal) reaction, which is thought to be a Th1-type cellular immune response and is characterized by an acute inflammatory reaction that causes worsening of skin lesions, neuritis and other systemic complications that occur in patients who are immunologically unstable [42]. Therefore, the increase in HSL expression detected in untreated BL patients is potentially activation of an immune reaction. The lepra reaction is one of the major problems faced by clinicians during treatment, and there is currently no method of predicting this critical side effect of treatment. Our observation suggests that detecting HSL mRNA in slit-skin smear samples from untreated patients could potentially be a reliable, convenient and minimally invasive procedure by which to predict possible occurrence of the type 1 lepra reaction. In addition, MDT treatment results in a rapid induction of HSL expression. Consequently, HSL expression levels after MDT treatment might also be a marker for treatment efficacy without the need for complicated tests to evaluate drug resistance of the bacilli. Although early diagnosis and appropriate treatment provide a complete cure, delays in diagnosis and treatment result in severe deformities and disabilities. Therefore, evaluation of HSL levels from slit-skin smear samples may be a simple and accurate method for clinical examination. In both cases, however, analysis of more clinical samples is needed to validate the clinical usefulness of this metric.

In conclusion, we have shown that *M. leprae* infection suppresses host HSL expression, which helps to retain the lipid-rich environment necessary for the survival of the pathogen within the phagosome. In addition, the measurement of HSL expression from slit-skin smears may be a useful diagnostic tool for patient prognosis.

Acknowledgments

This work was supported by a Grant-in-Aid for Scientific Research from the Ministry of Education, Culture, Sports, Science

and Technology of Japan (K.S. and N.I.) and by a Grant-in-Aid for Research on Emerging and Reemerging Infectious Diseases from the Ministry of Health, Labor, and Welfare of Japan (K.S. and N.I.).

References

[1] Global leprosy situation. Wkly Epidemiol Rec 2010;85:337–48.
[2] Ridley DS, Jopling WH. Classification of leprosy according to immunity. a five-group system. Int J Lepr Other Mycobact Dis 1966;34:255–73.
[3] Cardona PJ, Llatjos R, Gordillo S, Díaz J, Ojanguren I, Ariza A, et al. Evolution of granulomas in lungs of mice infected aerogenically with *Mycobacterium tuberculosis*. Scand J Immunol 2000;52:156–63.
[4] Kondo E, Kanai K. Accumulation of cholesterol esters in macrophages incubated with mycobacteria in vitro. Jpn J Med Sci Biol 1976;29:123–37.
[5] Blanchette-Mackie EJ, Dwyer NK, Barber T, Coxey RA, Takeda T, Rondinone CM, et al. Perilipin is located on the surface layer of intracellular lipid droplets in adipocytes. J Lipid Res 1995;36:1211–26.
[6] Brasaemle DL, Barber T, Wolins NE, Serrero G, Blanchette-Mackie EJ, Londos C. Adipose differentiation-related protein is an ubiquitously expressed lipid storage droplet-associated protein. J Lipid Res 1997;38:2249–63.
[7] Miura S, Gan JW, Brzostowski J, Parisi MJ, Schultz CJ, Londos C, et al. Functional conservation for lipid storage droplet association among perilipin, ADRP, and TIP47 (PAT)-related proteins in mammals, Drosophila, and Dictyostelium. J Biol Chem 2002;277:32253–7.
[8] Wolins NE, Rubin B, Brasaemle DL. TIP47 associates with lipid droplets. J Biol Chem 2001;276:5101–8.
[9] Tanigawa K, Suzuki K, Nakamura K, Akama T, Kawashima A, Wu H, et al. Expression of adipose differentiation-related protein (ADRP) and perilipin in macrophages infected with *Mycobacterium leprae*. FEMS Microbiol Lett 2008; 289:72–9.
[10] Zimmermann R, Lass A, Haemmerle G, Zechner R. Fate of fat: the role of adipose triglyceride lipase in lipolysis. Biochim Biophys Acta 2009;1791: 494–500.
[11] Garton AJ, Yeaman SJ. Identification and role of the basal phosphorylation site on hormone-sensitive lipase. Eur J Biochem 1990;191:245–50.
[12] Yogi Y, Banba T, Kobayashi M, Katoh H, Jahan N, Endoh M, et al. Leprosy in hypertensive nude rats (SHR/NCrj-*rnu*). Int J Lepr Other Mycobact Dis 1999; 67:435–45.
[13] Yogi Y, Endoh M, Banba T, Kobayashi M, Katoh H, Suzuki K, et al. Susceptibility to *Mycobacterium leprae* of congenic hypertensive nude rat (SHR/NCrj-*rnu*) and production of cytokine from the resident peritoneal macrophages. Jpn J Lep 2002;71:39–45.
[14] Akama T, Suzuki K, Tanigawa K, Kawashima A, Wu H, Nakata N, et al. Whole-genome tiling array analysis of *Mycobacterium leprae* RNA reveals high expression of pseudogenes and noncoding regions. J Bacteriol 2009;191: 3321–7.
[15] Akama T, Tanigawa K, Kawashima A, Wu H, Ishii N, Suzuki K. Analysis of *Mycobacterium leprae* gene expression using DNA microarray. Microb Pathog 2010;49:181–5.
[16] Suzuki K, Takeshita F, Nakata N, Ishii N, Makino M. Localization of CORO1A in the macrophages containing *Mycobacterium leprae*. Acta Histochem Cytochem 2006;39:107–12.
[17] Tanigawa K, Suzuki K, Kimura H, Takeshita F, Wu H, Akama T, et al. Tryptophan aspartate-containing coat protein (CORO1A) suppresses Toll-like receptor signalling in *Mycobacterium leprae* infection. Clin Exp Immunol 2009;156:495–501.
[18] Ferrari G, Langen H, Naito M, Pieters J. A coat protein on phagosomes involved in the intracellular survival of mycobacteria. Cell 1999;97:435–47.
[19] Su CL, Sztalryd C, Contreras JA, Holm C, Kimmel AR, Londos C. Mutational analysis of the hormone-sensitive lipase translocation reaction in adipocytes. J Biol Chem 2003;278:43615–9.
[20] Anthonsen MW, Ronnstrand L, Wernstedt C, Degerman E, Holm C. Identification of novel phosphorylation sites in hormone-sensitive lipase that are phosphorylated in response to isoproterenol and govern activation properties in vitro. J Biol Chem 1998;273:215–21.
[21] Krutzik SR, Ochoa MT, Sieling PA, Uematsu S, Ng YW, Legaspi A, et al. Activation and regulation of Toll-like receptors 2 and 1 in human leprosy. Nat Med 2003;9:525–32.
[22] Cole ST, Eiglmeier K, Parkhill J, James KD, Thomson NR, Wheeler PR, et al. Massive gene decay in the leprosy bacillus. Nature 2001;409:1007–11.
[23] Hunter RL, Jagannath C, Actor JK. Pathology of postprimary tuberculosis in humans and mice: contradiction of long-held beliefs. Tuberculosis 2007;87: 267–78.
[24] Peyron P, Vaubourgeix J, Poquet Y, Levillain F, Botanch C, Bardou F, et al. Foamy macrophages from tuberculous patients' granulomas constitute a nutrient-rich reservoir for *M. tuberculosis* persistence. PLoS Pathogens 2008; 4:e1000204.
[25] van der Wel N, Hava D, Houben D, Fluitsma D, van Zon M, Pierson J, et al. *M. tuberculosis* and *M. leprae* translocate from the phagolysosome to the cytosol in myeloid cells. Cell 2007;129:1287–98.
[26] Kim MJ, Wainwright HC, Locketz M, Bekker LG, Walther GB, Dittrich C, et al. Caseation of human tuberculosis granulomas correlates with elevated host lipid metabolism. EMBO Mol Med 2010;2:258–74.
[27] Welin A, Lerm M. Inside or outside the phagosome? the controversy of the intracellular localization of *Mycobacterium tuberculosis*. Tuberculosis; 2011.
[28] Sakurai I, Skinsnes OK. Lipids in leprosy. 2. histochemistry of lipids in human leprosy. Int J Lepr Other Mycobact Dis 1970;38:389–403.
[29] Ridley MJ, Ridley DS, De Beer FC, Pepys MB. C-reactive protein and apoB containing lipoproteins are associated with *Mycobacterium leprae* in lesions of human leprosy. Clin Exp Immunol 1984;56:545–52.
[30] Chan J, Fujiwara T, Brennan P, McNeil M, Turco SJ, Sibille JC, et al. Microbial glycolipids: possible virulence factors that scavenge oxygen radicals. Proc Natl Acad Sci U S A 1989;86:2453–7.
[31] Cruz D, Watson AD, Miller CS, Montoya D, Ochoa MT, Sieling PA, et al. Host-derived oxidized phospholipids and HDL regulate innate immunity in human leprosy. J Clin Invest 2008;118:2917–28.
[32] Navab M, Ananthramaiah GM, Reddy ST, Van Lenten BJ, Ansell BJ, Fonarow GC, et al. The oxidation hypothesis of atherogenesis: the role of oxidized phospholipids and HDL. J Lipid Res 2004;45:993–1007.
[33] Ogasawara J, Nomura S, Rahman N, Sakurai T, Kizaki T, Izawa T, et al. Hormone-sensitive lipase is critical mediators of acute exercise-induced regulation of lipolysis in rat adipocytes. Biochem Biophys Res Commun 2010;400:134–9.
[34] Sztalryd C, Xu G, Dorward H, Tansey JT, Contreras JA, Kimmel AR, et al. Perilipin A is essential for the translocation of hormone-sensitive lipase during lipolytic activation. J Cell Biol 2003;161:1093–103.
[35] Subramanian V, Rothenberg A, Gomez C, Cohen AW, Garcia A, Bhattacharyya S, et al. Perilipin A mediates the reversible binding of CGI-58 to lipid droplets in 3T3-L1 adipocytes. J Biol Chem 2004;279:42062–71.
[36] Large V, Reynisdottir S, Langin D, Fredby K, Klannemark M, Holm C, et al. Decreased expression and function of adipocyte hormone-sensitive lipase in subcutaneous fat cells of obese subjects. J Lipid Res 1999;40:2059–66.
[37] Jocken JW, Langin D, Smit E, Saris WH, Valle C, Hul GB, et al. Adipose triglyceride lipase and hormone-sensitive lipase protein expression is decreased in the obese insulin-resistant state. J Clin Endocrinol Metab 2007; 92:2292–9.
[38] Kim JY, Tillison K, Lee JH, Rearick DA, Smas CM. The adipose tissue triglyceride lipase ATGL/PNPLA2 is downregulated by insulin and TNF-alpha in 3T3-L1 adipocytes and is a target for transactivation by PPARgamma. Am J Physiol Endocrinol Metab 2006;291:E115–27.
[39] Kralisch S, Klein J, Lossner U, Bluher M, Paschke R, Stumvoll M, et al. Isoproterenol, TNFalpha, and insulin downregulate adipose triglyceride lipase in 3T3-L1 adipocytes. Mol Cell Endocrinol 2005;240:43–9.
[40] Sano K, Tomioka H, Sato K, Sano C, Kawauchi H, Cai S, et al. Interaction of antimycobacterial drugs with the anti-*Mycobacterium avium* complex effects of antimicrobial effectors, reactive oxygen intermediates, reactive nitrogen intermediates, and free fatty acids produced by macrophages. Antimicrob Agents Chemother 2004;48:2132–9.
[41] Brzostek A, Pawelczyk J, Rumijowska-Galewicz A, Dziadek B, Dziadek J. *Mycobacterium tuberculosis* is able to accumulate and utilize cholesterol. J Bacteriol 2009;191:6584–91.
[42] Sasaki S, Takeshita F, Okuda K, Ishii N. *Mycobacterium leprae* and leprosy: a compendium. Microbiol Immunol 2001;45:729–36.

doi: 10.1111/j.1346-8138.2011.01355.x

CASE REPORT

Mycobacterium shigaense sp. nov., a novel slowly growing scotochromogenic mycobacterium that produced nodules in an erythroderma patient with severe cellular immunodeficiency and a history of Hodgkin's disease

Kazue NAKANAGA,[1] Yoshihiko HOSHINO,[1] Makiko WAKABAYASHI,[2] Noriki FUJIMOTO,[2] Enrico TORTOLI,[3] Masahiko MAKINO,[1] Toshihiro TANAKA,[2] Norihisa ISHII[1]

[1]Leprosy Research Center, National Institute of Infectious Diseases, Tokyo, [2]Department of Dermatology, Shiga University of Medical Science, Shiga, Japan; and [3]Regional Reference Center for Mycobacteria, Careggi University Hospital, Florence, Italy

ABSTRACT

A novel slow-growing scotochromogenic mycobacterium was isolated from skin biopsies from a patient with a history of Hodgkin's disease and severe cellular immunodeficiency as an opportunistic pathogen. Clinical characterization of these lesions revealed papules and nodules with pathological granuloma formation. Genotypic analysis using 16S rRNA misidentified this isolate as *Mycobacterium simiae*. However, multiple gene analysis using the internal transcribed spacer between the 16S and 23S rRNA genes, and the *rpoB* and *hsp65* genes revealed the presence of a novel mycobacterium. The antimicrobial susceptibility of this isolate was completely different from that of *M. simiae*. On the basis of these findings, we propose naming this new species *Mycobacterium shigaense* sp. nov., and conclude that multiple gene analysis is required for the appropriate diagnosis and treatment of non-tuberculous mycobacterial infections.

Key words: cellular immunodeficiency, *Mycobacterium shigaense* sp.nov., non-tuberculous mycobacteria, opportunistic infection.

INTRODUCTION

Non-tuberculous mycobacteria (NTM) have been well recognized as causative agents of human diseases. Recently, a number of new species have been added to the NTM. Some of these cause opportunistic infections in immunocompromised patients, not only those with AIDS, but also non-AIDS associated infections. Here, we report an additional new species of mycobacterium that caused cutaneous infection occurring as an opportunistic infection.

CASE REPORT

A 55-year-old Japanese male with a history of treatment of neck-oriented Hodgkin's disease in 2000, presented with erythema accompanied by generalized itching in 2005. The lesion persisted and worsened after treatment with a low dose of oral corticosteroids, resulting in erythroderma and scattered cutaneous nodules on the body trunk in 2007. On physical examination, he presented with itchy erythema over more than 90% of the total body surface (erythroderma) (Fig. 1a); scattered nodules on his chest, back and extremities (Fig. 1b); and multiple papules (Fig. 1c) on his back. He also presented with high-grade fever and slight lymphadenopathy of the neck and axilla. Cytomegalovirus (CMV) retinitis was diagnosed by ophthalmologists and several positive values of CMV antigen were detected at the end stage. His symptoms progressed, and after 2008 he was treated with ganciclovir or valganciclovir. Laboratory tests showed elevated levels of white blood cells ($10.2 \times 10^3/mm^3$; normal range [NR], $3.0–8.0 \times 10^3$) composed of 79.8% segmented neutrophils (NR, 40–74), 3.9% eosinophils (NR, 0–7), 11% lymphocytes (NR, 15–48) and 0% atypical lymphocytes, lactate dehydrogenase (295 IU/L; NR, 100–210), C-reactive protein (1.9 mg/dL; NR, <0.3), immunoglobulin E (188 498 IU/mL; NR, <400) and soluble interleukin-2 receptor (7470 U/mL; NR, 135–483). The platelet counts, liver and renal functions, serum immunoglobulin levels, complement values and angiotensin-converting enzyme were all within normal ranges. Antibodies against human T-lymphotropic virus-1 and HIV-1 were negative. Phenotypic analysis of peripheral lymphocytes revealed an increase in CD3 (95%; NR, 60–78%), T-cell receptors (TCR)-αβ (94%) and -γδ (1%), CD4 (93%; NR, 28–47) CD8 (3%; NR, 25–42) and CD19 (1%; NR, 6–16). Southern blot of peripheral lymphocytes revealed no monoclonal band. A tuberculin skin test for purified protein derivative was

Correspondence: Kazue Nakanaga, Ph.D., Department of Mycobacteriology, Leprosy Research Center, National Institute of Infectious Diseases, 4-2-1 Aoba-cho, Higashimurayama-shi, Tokyo 189-0002, Japan. Email: nakanaga@nih.go.jp

Received 24 April 2011; accepted 21 June 2011.

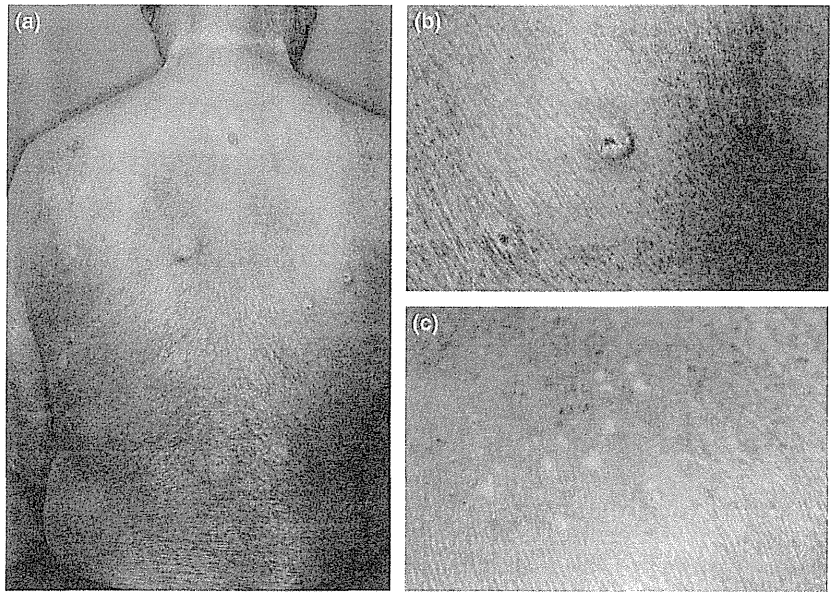

Figure 1. (a) Itchy erythema covered more than 90% of the body surface. (b) Scattered cutaneous nodules on the trunk. (c) Multiple papules on the back.

negative. A systemic investigation using computed tomography, endoscopy and Gallium scintigraphy revealed no abnormalities or internal malignancies, including a recurrence of Hodgkin's disease.

Skin biopsies were taken from the erythema, nodules and papules. A biopsy specimen from the erythema showed only lymphocytic infiltration (primarily CD4 T cells) around superficial dermal vessels (Fig. 2a). The lymphocytes were histologically normal, and Southern blot analysis of the biopsy specimen revealed no monoclonal band. The papules were histologically diagnosed as molluscum contagiosum (MC), because numerous basophilic inclusion bodies were observed in keratinocytes which located in the upper dermis. The nodular lesions showed dense infiltration of histiocytes in the superficial dermis, which formed granulomatous lesions (Fig. 2b). Ziehl–Neelsen staining of repeated biopsy specimens from these nodules showed multiple copies of banded acid-fast bacilli (Fig. 2c).

From these findings, we initially diagnosed an opportunistic mycobacterium infection in a patient of cellular immunodeficiency and administrated 400 mg of oral clarithromycin and 400 mg of isoniazid daily. The nodules improved within a few weeks. Multiple biopsies and histological investigations with Ziehl–Neelsen staining failed to detect any bacilli. The medicines were administrated for 12 months. New lesions of MC sometimes occurred after cessation of drug therapy, but no nodules were found. Oral prednisolone was administrated for the erythroderma. The erythroderma often recurred after healing of the mycobacterial infection, but because none of the skin biopsies from the erythroderma and peripheral blood showed atypical cells, the origin of the erythroderma is unknown.

While oral corticosteroids were effective, a daily low dose was needed to control the erythroderma. In October 2009, he complained of abdominal pain. At the time, he was almost blind due to CMV retinitis. Computed tomography showed a mass in the small

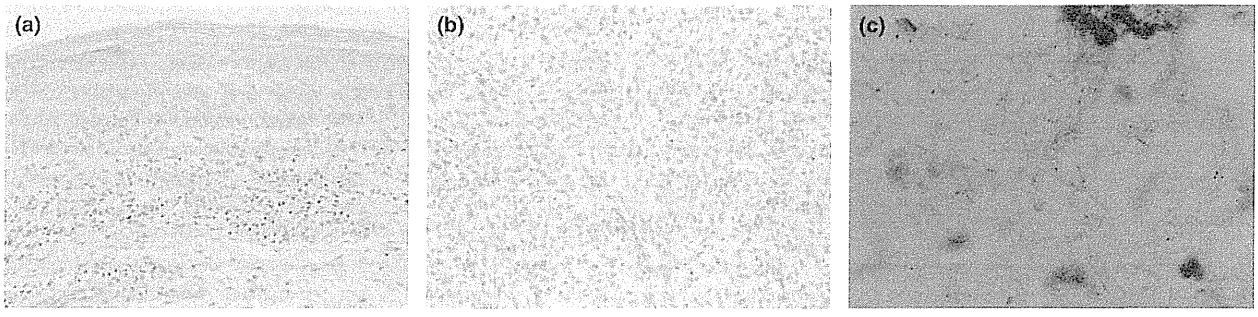

Figure 2. (a) Histological examination of erythema. Lymphocytic infiltration around superficial dermal vessels (hematoxylin–eosin [HE], original magnification ×100). (b) Histological examination of nodular lesions. Dense infiltrated histiocytes formed granulomatous lesions in the dermis (HE, ×200). (c) Ziehl–Neelsen staining of a skin biopsy from a nodule (oil immersion, ×1000).

intestine and perforation of the gastrointestinal tract. Although a surgical resection of the mass in the small intestine was performed, he died of sepsis in November 2009. An autopsy was not performed. However, a histopathological examination of the mass revealed dense atypical lymphocytic infiltration without Hodgkin's cells, and Southern blot analysis showed a monoclonal band of TCR-αβ cells. Therefore, we concluded that he died not of a recurrence of Hodgkin's disease, but of non-Hodgkin T-cell lymphoma (NHL) with severe immunodeficiency.

A skin biopsy from the nodules confirmed multiple copies of acid-fast bacilli with Ziehl–Neelsen staining, although polymerase chain reaction (PCR) tests targeting *Mycobacterium tuberculosis*, *Mycobacterium avium*, *Mycobacterium intracellulare* and *Mycobacterium leprae* were all negative. The sequencing and genotypic analysis of DNA from the biopsy specimens using the first one-third of the16S rRNA gene showed the highest similarities to *Mycobacterium simiae* (99.54% identity with a 2-bp difference) and *Mycobacterium interjectum* (98.61% identity with a 6-bp difference) when compared with the Ribosomal Differentiation of Micro-organisms (RIDOM) database.[1]

The mycobacterium was isolated from the skin biopsy using the BBL MGIT tube (Becton Dickinson, Franklin Lakes, NJ, USA) and designated *Mycobacterium* sp. UN-152. Phenotypic characteristics were analyzed after sub-culturing on 2% Ogawa egg slant medium (Table 1).[2] The strain was scotochromogenic with an intense yellow color in both light and dark conditions and had a banded appearance after Ziehl–Neelsen staining (Fig. 3), however, usual strains of *M. simiae* are photochromogenic. The strain was slow-growing, had a smooth colonial morphology, and was positive for 3-day arylsulfatase activity, 68°C and semi-quantitative catalase activity

Table 1. Phenotypic differentiation between isolate *Mycobacterium* sp. UN-152 and genotypically similar species of mycobacteria

Characteristics	Isolate UN152 of *Mycobacterium* sp.	*Mycobacterium simiae* ATCC 25275^T	*Mycobacterium interjectum* ATCC 51457^T
Growth† in 7 days	+	+	+
Growth† at:			
25°C	+	+	+
30°C	+	+	+
37°C	+	+	+
42°C	–	+	–
Colony morphology	Smooth	Smooth	Smooth
Colony pigmentation			
In the dark	+	–	+
Photoactivity	–	+	–
Growth† supplemented with:			
PNB (500 μg/mL)	+	+	+
NaCl (5%)	+	+	+
TCH (1 μg/mL)	+	+	+
TCH (10 μg/mL)	+	+	+
Iron uptake	–	–	–
Niacin	–	+	–
Tween-80 hydrolysis (5, 10 days)	–	–	–
Urease	+	+	+
Nitrate reduction	–	–	–
Semi-quantitative catalase	+	+	+
68°C catalase	+	+	+
Arylsulfatase (3 day)	+	–	–
Pyrazinamidase	+	+	+
MPB64 production	–	–	–

†Bacterial growth was examined on 2% Ogawa slants.

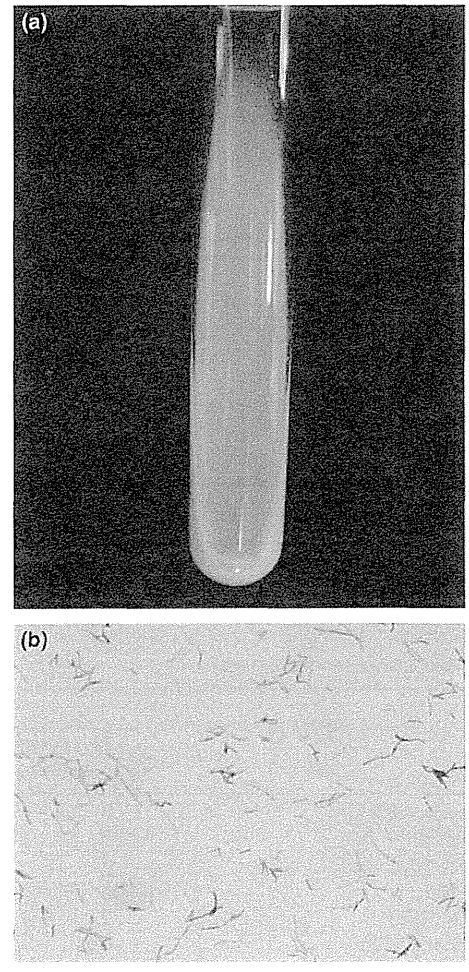

Figure 3. (a) Scotochromogenic colonies of *Mycobacterium* sp. UN-152 sub-cultured on 2% Ogawa egg medium. (b) Ziehl–Neelsen staining of *Mycobacterium* sp. UN-152 sub-cultured on 2% Ogawa egg medium (oil immersion, ×1000).

and urease activity, but was negative for niacin activity, which suggested that this isolate was phenotypically different from *M. simiae*.

DNA–DNA hybridization to identify the species (DDH Mycobacteria Kyokuto Pharmaceutical Industrial, Tokyo, Japan) produced no matches with any of the 18 mycobacteria species included in the panel with *M. simiae*.[3] Further genotypic analysis was performed in an attempt to identify this isolate. Sequence analysis targeting fragments of the 16S rRNA gene, the internal transcribed spacer between the 16S and 23S rRNA genes (ITS region), and the *rpoB* and *hsp65* genes was performed (Table 2). Amplified PCR products were sequenced using an ABI Prism 310 PCR Genetic Analyzer (Applied Biosystems, Foster City, CA).[8] The sequences of isolate UN-152 were compared to those from the *M. simiae* (ATCC25275^T) type strain and the *M. simiae* clinical isolate 51808 from Japan.[9] We also performed a similarity search using BLAST to find identical and/or closely-related species of mycobacteria.[10] Phylogenetic analyses were performed using the neighbor joining method with Kimura's two-parameter distance correction model with 1000 bootstrap replications in the MEGA version 4.0.2 (Build#: 4028) software package.[11]

The sequence of the first one-third of the 16S rRNA gene from a sub-culture was identical with that from the previously examined skin biopsy. There were only four sites of a point difference between the sequence of UN-152 and that of *M. simiae* (99.7%

Table 2. Primers used in this study

Primer	Sequence	Target (amplified fragment size)	Reference
8F16S	5′-AGAGTTTGATCCTGGCTCAG-3′	16S rRNA gene (~1500 bp)	4
1047R16S	5′-TGCACACAGGCCACAAGGGA-3′		
830F16S	5′-GTGTGGGTTTCCTTCCTTGG-3′		
1542R16S	5′-AAGGAGGTGATCCAGCCGCA-3′		
ITSF	5′-TTGTACACACCGCCCGTC-3′	16S-23S ITS region (~340 bp)	5
ITSR	5′-TCTCGATGCCAAGGCATCCACC-3′		
MF	5′-CGACCACTTCGGCAACCG-3′	*rpoB* gene (351 bp)	6
MR	5′-TCGATCGGGCACATCCGG-3′		
TB11	5′-ACCAACGATGGTGTGTCCAT-3′	*hsp65* gene (441 bp)	7
TB12	5′-CTTGTCGAACCGCATACCCT-3′		

Table 3. DNA sequence similarities between isolate *Mycobacterium* sp. UN-152 and highly similar species of mycobacteria

	% identity			
Species†	16S rRNA (1471 bp)	ITS (280 bp)	*rpoB* (315 bp)	*hsp65* (401 bp)
Mycobacterium sp. UN-152	100	100	100	100
Mycobacterium simiae ATCC 25275^T	99.7	88.4	90.2	94.0
M. simiae 051808	99.7	88.4	90.8	94.0
Mycobacterium sherrisii ATCC BAA-832^T	99.5	ND	ND‡	93.0
Mycobacterium triplex ATCC 700071^T	99.1	85.7	ND	94.3
Mycobacterium cookii CIP 105396^T	ND	ND	95.9	93.3

†Sequence data (accession number in parenthesis) of three species were taken from database: *M. sherrisii* (AY353699, AY365190), *M. triplex* (U57632, GQ153291, AF334028) and *M. cookii* (AF547824, AY544904). ‡Not determined.

Table 4. Antibiotic susceptibility tests

	Minimal inhibitory concentration (μg/mL)		
Antibiotics	Isolate UN152 of *Mycobacterium* sp.	*Mycobacterium simiae* isolate	*M. simiae* (ATCC 25275T)
Streptomycin (SM)	8	16	4
Ethambutol (EB)	>128	32	44
Kanamycin (KM)	4	8	4
Isoniazid (INH)	>32	32	4
Rifampicin (REF)	0.03	>32	>32
Levofloxacin (LVFX)	0.5	2	1
Clarithromycin (CAM)	1	8	2
Ethionamide (TH)	>16	4	4
Amikacin (AMK)	4	8	4

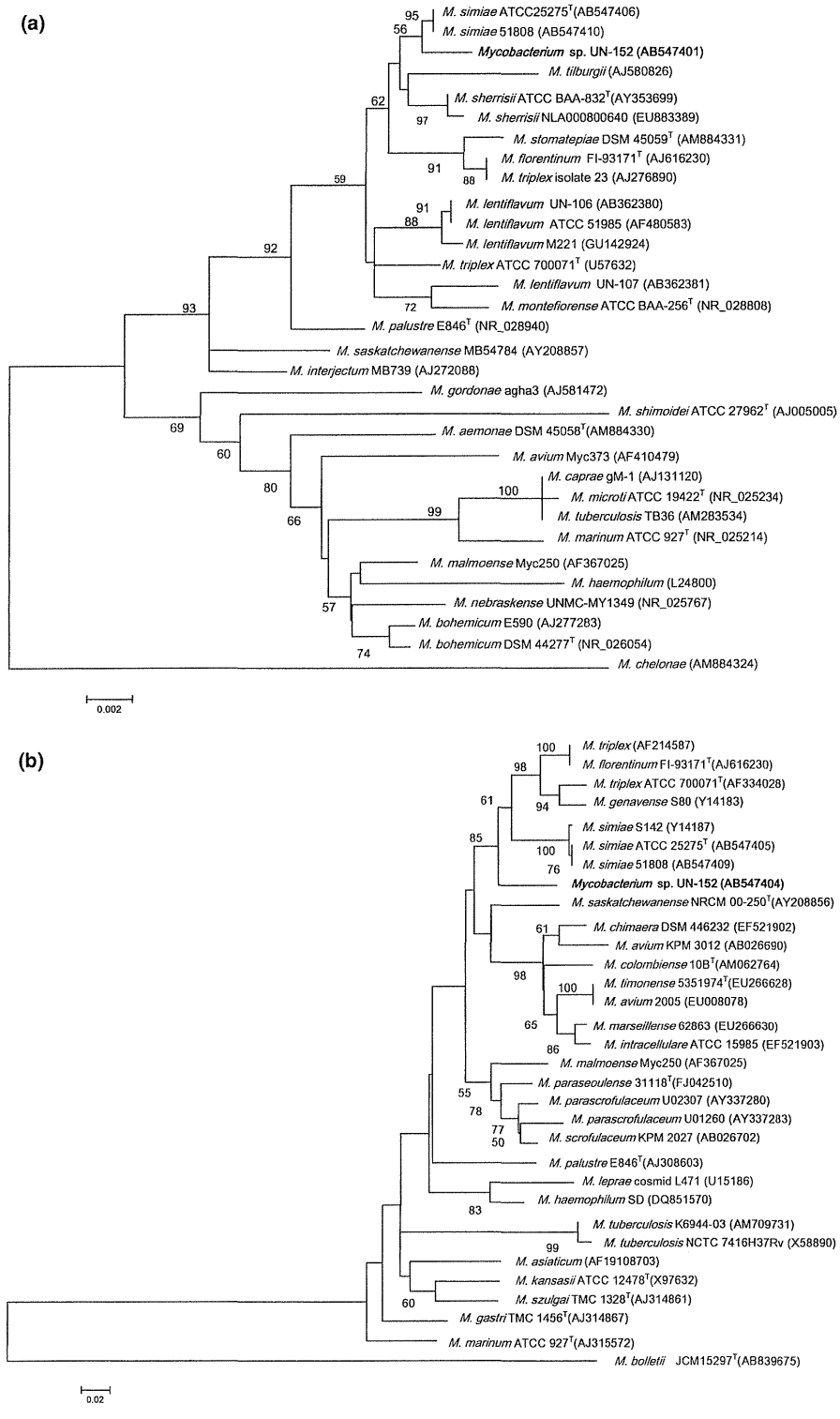

Figure 4. (a) Phylogenetic position of *Mycobacterium* sp. UN-152 (bold font) based on 1471 bp of the 16S rRNA gene. The percentages at the nodes represent bootstrap levels (values of <50% are not shown). The scale bar represents differences in nucleotide sequences. (b) Phylogenetic position of *Mycobacterium* sp. UN-152 (bold font) based on 280 bp of the 16S-23S rRNA ITS region. (c) Phylogenetic position of *Mycobacterium* sp. UN-152 (bold font) based on 315 bp of the *rpoB* gene. (d) Phylogenetic position of *Mycobacterium* sp. UN-152 (bold font) based on 401 bp of the *hsp65* gene.

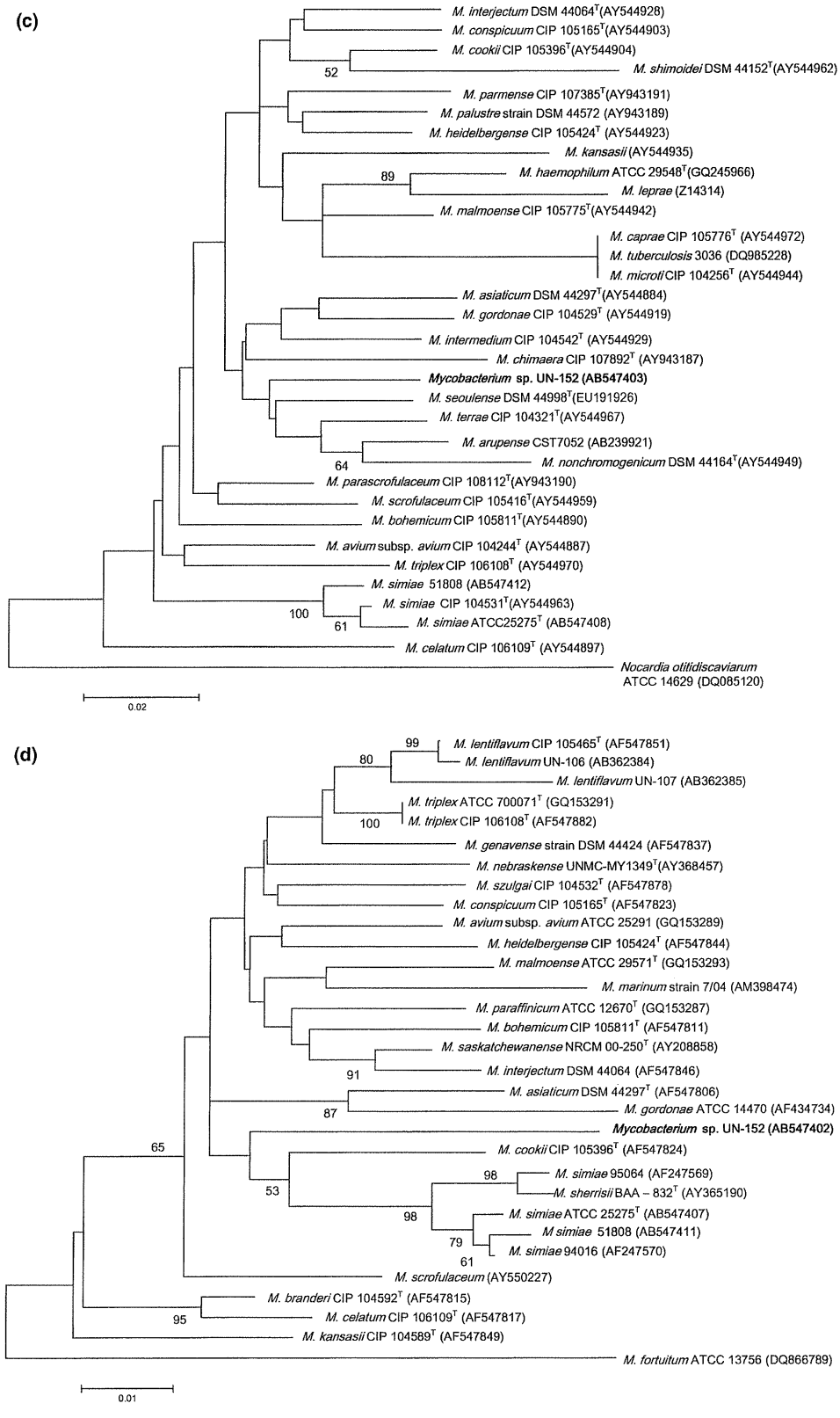

Figure 4. (*Continued*).

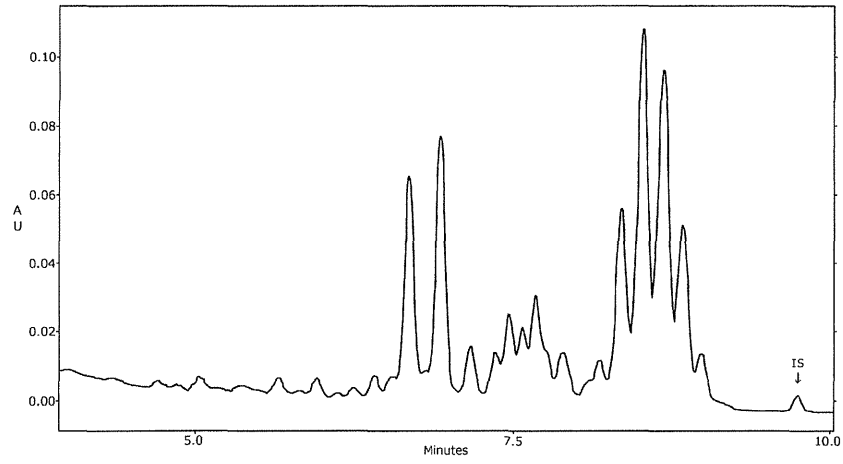

Figure 5. Mycolic acid analysis in *Mycobacterium* sp. UN-152 using high-performance liquid chromatography. IS, high molecular mass internal standard.

identity) when compared to almost all portions of the 16S rRNA gene (1471 bp). In contrast, the sequence identity of the ITS region was only 88. 4% between UN-152 and the *M. simiae*. *Mycobacterium cookii* revealed the highest similarity (95.9% identity) in the *rpoB* gene while *M. simiae* showed only 90.2–90.8% identities. *Mycobacterium triplex* exhibited the highest similarity in the *hsp65* gene (94.3% identity) while *M. simiae* was 94.0% similar (Table 3). However, there was no single mycobacterium species that showed the highest similarity across these four gene fragments, which suggested that this clinical isolate, *Mycobacterium* sp. UN-152, was a novel mycobacterium (Fig. 4).

Table 4 shows the results of antimicrobial susceptibility tests against *Mycobacterium* sp. UN-152, and the two strains of *M. simiae* (BrothMIC NTM; Kyokuto Pharmaceutical Industrial). *Mycobacterium* sp. UN-152 was highly susceptible to rifampicin and exhibited good susceptibility to clarithromycin and levofloxacin. Conversely, the minimal inhibitory concentration of rifampicin to *M. simiae* reference and clinical strains was more than 32 μg/mL, demonstrating that the antimicrobial susceptibility profile of the unknown isolate was different from that of *M. simiae*. The sequences obtained from the multiple gene analysis of the unknown clinical isolate (*Mycobacterium* sp. UN-152) and the *M. simiae* reference strains (ATCC25275^T and 51808) were deposited into the International Nucleotide Sequence Databases (INSD) through the DNA Databank of Japan (DDBJ)[12] under the accession numbers AB547401 to AB547412.

Finally, high-performance liquid chromatography of mycolic acid methyl esters was performed according to the CDC guidelines.[13] The pattern of bromophenacyl esters of mycolic acids can be used as an alternative method of discrimination of mycobacteria. The chromatographs revealed a representative profile characterized by three late clusters of peaks grossly resembling *M. simiae* or *Mycobacterium lentiflavum* (Fig. 5).[14]

DISCUSSION

Based on colony morphology, this clinical isolate may belong to NTM Runyon II. Because a slow-growing mycobacterium has a long culture time, the genotypic analysis of clinical samples would enable rapid diagnosis and treatment.[8,15] Genotypic analysis using the 16S rRNA gene is now contributing to diagnostics as an identification methodology for novel NTM.[16] In this case, the result of 16S rRNA gene sequences strongly suggested that *M. simiae* was the etiological strain; however, the identification was not supported by the scotochromogenic colony morphology and negative niacin accumulation. Additional sequence analysis targeting the ITS region and the *rpoB* and *hsp65* genes suggested the different species of mycobacteria, leading to the discovery of a novel NTM. We propose naming this new species *Mycobacterium shigaense* sp. nov.

Some species of recently registered mycobacteria may be of dubious clinical significance.[16] This isolate was determined to be clinically significant and not an environmental contaminant because: (i) it was isolated from multiple nodules, not from the erythema; (ii) the nodules improved after treatment with clarithromycin and isoniazid; and (iii) the isolate was no longer detectable once the nodules improved, a result which was repeatedly confirmed histologically. Unfortunately we could not know the source of this mycobacterium infection from medical interview.

In this case, MC infection was frequently seen in the trunk, CMV retinitis was diagnosed and treated for several months, and finally NHL was diagnosed. These findings were indicative of a significant cellular immunity deficiency because MC, CMV and NHL are frequently found in advanced AIDS patients with significant cellular immunodeficiency.[17–19] We propose that the decrease of peripheral CD8 T cells and the history of Hodgkin's disease resulted in severe immunodeficiency and that the cutaneous *M. shigaense* infection occurred as an opportunistic infection.

The genotypes obtained from a skin biopsy and subculture were identical, suggesting that the bacterium is responsible for the multiple nodules. In addition to the clinical significance, this case shows the insufficiency of single 16S rRNA gene analysis. Multiple gene analysis would be required to identify the species of mycobacteria.[20] This species has been never reported, but may have been previously misidentified as *M. simiae*. Because *M. shigaense* and *M. simiae* differ significantly in their susceptibility to rifampicin,

clinicians must differentiate the two isolates in terms of the treatment. Therefore, multiple gene analysis that includes the ITS region and *rpoB* and *hsp65* genes is required for the appropriate treatment and diagnosis of NTM.

ACKNOWLEDGMENTS

We are indebted to Dr Tatsuo Kato (Nagara Medical Center) for giving us a clinical isolate of *Mycobacterium simiae* 51808. This work was supported in part by a Grant-in-Aid for Research on Emerging and Re-emerging Infectious Diseases from the Ministry of Health, Labor and Welfare of Japan to Y. H., M. M. and N. I. and by a Grant-in-Aid for Scientific Research (C) from the Ministry of Education, Culture, Sports, Science and Technology of Japan to Y. H.

REFERENCES

1 Turenne CY, Tschetter L, Wolfe J *et al.* Necessity of quality-controlled 16S rRNA gene sequence databases: identifying nontuberculous *Mycobacterium* species. *J Clin Microbiol* 2001; **39**: 3637–3648.
2 Della-Latta P, Weitzman I. Mycobacteriology. In: Isenberg HD, ed. *Essential Procedures for Clinical Microbiology*, 1st edn. Washington, DC: ASM Press, 1998; 169–203.
3 Kusunoki S, Ezaki M, Tamesada Y *et al.* Application of colorimetric microdilution plate hybridization for rapid genetic identification of 22 *Mycobacterium* species. *J Clin Microbiol* 1991; **29**: 1596–1603.
4 Springer B, Wu WK, Bodmer T *et al.* Isolation and characterization of a unique group of slowly growing mycobacteria: description of *Mycobacterium lentiflavum* sp. nov. *J Clin Microbiol* 1996; **34**: 1100–1107.
5 Roth A, Fischer M, Hamid ME *et al.* Differentiation of phylogenetically related slowly growing mycobacteria based on 16S–23S rRNA gene internal transcribed spacer sequences. *J Clin Microbiol* 1998; **36**: 139–147.
6 Kim B-J, Lee S-H, Lyu M-A *et al.* Identification of mycobacterial species by comparative sequence analysis of the RNA polymerase gene (*rpoB*). *J Clin Microbiol* 1999; **37**: 1714–1720.
7 Telenti A, Marchesi F, Balz M *et al.* Rapid identification of mycobacteria to the species level by polymerase chain reaction and restriction enzyme analysis. *J Clin Microbiol* 1993; **31**: 175–178.
8 Nakanaga K, Ishii N, Suzuki K *et al.* "*Mycobacterium ulcerans* subsp. *shinshuense*" isolated from a skin ulcer lesion: identification based on 16S rRNA gene sequencing. *J Clin Microbiol* 2007; **45**: 3840–3843.
9 Yoshimura K, Imao M, Goto H *et al.* A case of pulmonary infection due to *Mycobacterium simiae*. *Nihon Kokyuki Gakkai Zasshi* 2005; **43**: 32–36.
10 Altschul SF, Madden TL, Schaffer AA *et al.* Gapped BLAST and PSI-BLAST: a new generation of protein database search programs. *Nucleic Acids Res* 1997; **25**: 3389–3402.
11 Tamura K, Dudley J, Nei M *et al.* MEGA4: Molecular Evolutionary Genetics Analysis (MEGA) software version 4.0. *Mol Biol Evol* 2007; **24**: 1596–1599.
12 Kaminuma E, Mashima J, Kodama Y, *et al.* DDBJ launches a new archive database with analytical tools for next-generation sequence data. *Nucleic Acids Res* 2010; **38**: Database issue D33–D38.
13 Butler WR, Margaret MS, Floyd M, *et al.* Standardized method for HPLC identification of mycobacteria. 1996 [WWW document]. [cited 20 Apr, 2011] Available from URL: www.cdc.gov/ncidod/publications/hplc.pdf.
14 Tortoli E, Bartoloni A. High-performance liquid chromatography and identification of mycobacteria. *Rev Med Microbiol* 1996; **7**: 207–219.
15 Ishiwada N, Hishiki H, Watanabe M *et al.* Usefulness of PCR in rapidly diagnosing subcutaneous abscess and costal osteomyelitis caused by *Mycobacterium bovis* BCG. *Kansenshogaku Zasshi* 2008; **82**: 30–33.
16 Griffith DE, Aksamit T, Brown-Elliott BA *et al.* An official ATS/IDSA statement: diagnosis, treatment, and prevention of nontuberculous mycobacterial diseases. *Am J Respir Crit Care Med* 2007; **175**: 367–416.
17 Hoshino Y, Nagata Y, Gatanaga H *et al.* Cytomegalovirus (CMV) retinitis and CMV antigenemia as a clue to impaired adrenocortical function in patients with AIDS. *AIDS* 1997; **11**: 1719–1724.
18 Hoshino Y, Nagata Y, Taguchi H *et al.* Role of the cytomegalovirus (CMV)-antigenemia assay as a predictive and follow-up detection tool for CMV disease in AIDS patients. *Microbiol Immunol* 1999; **43**: 959–965.
19 Jung AC, Paauw DS. Diagnosing HIV-related disease: using the CD4 count as a guide. *J Gen Intern Med* 1998; **13**: 131–136.
20 Devulder G, Pérouse de Montclos M, Flandrois JP. A multigene approach to phylogenetic analysis using the genus Mycobacterium as a model. *Int J Syst Evol Microbiol* 2005; **55**: 293–302.

International Immunology, Vol. 24, No. 10, pp. 637–644
doi:10.1093/intimm/dxs062
Advance Access publication 13 June 2012

Critical role of AIM2 in *Mycobacterium tuberculosis* infection

Hiroyuki Saiga[1,2], Shoko Kitada[1], Yosuke Shimada[1,3], Naganori Kamiyama[1,3], Megumi Okuyama[1,3], Masahiko Makino[4], Masahiro Yamamoto[1,5,6,7] and **Kiyoshi Takeda[1,3,6]**

[1]Laboratory of Immune Regulation, Department of Microbiology and Immunology, Graduate School of Medicine, Osaka University, Suita, Osaka 565-0871, Japan
[2]The Association for Preventive Medicine of Japan, Koto-ku, Tokyo 135-0001, Japan
[3]Laboratory of Mucosal Immunology, WPI Immunology Frontier Research Center, Osaka University, Suita, Osaka 565-0871, Japan
[4]Department of Mycobacteriology, Leprosy Research Center, National Institute of Infectious Diseases, Higashimurayama, Tokyo 189-0002, Japan
[5]Laboratory of Immunoparasitology, WPI Immunology Frontier Research Center, Osaka University, Suita, Osaka 565-0871, Japan
[6]Core Research for Evolutional Science and Technology, Japan Science and Technology Agency, Saitama 332-0012, Japan
[7]Department of Immunoparasitology, Research Institute for Microbial Diseases, Osaka University, Suita, Osaka 565-0871, Japan

Correspondence to: K. Takeda; E-mail: ktakeda@ongene.med.osaka-u.ac.jp

Received 1 March 2012, *accepted* 9 April 2012

Abstract

Absent in melanoma 2 (AIM2) is a sensor of cytosolic DNA that is responsible for activation of the inflammasome and host immune responses to DNA viruses and intracellular bacteria. However, the role of AIM2 in host defenses against *Mycobacterium tuberculosis* is unknown. Here, we show that AIM2-deficient mice were highly susceptible to intratracheal infection with *M. tuberculosis* and that this was associated with defective IL-1β and IL-18 production together with impaired T_h1 responses. Macrophages from AIM2-deficient mice infected with *M. tuberculosis* showed severely impaired secretion of IL-1β and IL-18 as well as activation of the inflammasome, determined by caspase-1 cleavage. Genomic DNA extracted from *M. tuberculosis* (Mtb DNA) induced caspase-1 activation and IL-1β/IL-18 secretion in an AIM2-dependent manner. Mtb DNA, which was present in the cytosol, co-localized with AIM2. Taken together, these findings demonstrate that AIM2 plays an important role in *M. tuberculosis* infection through the recognition of Mtb DNA.

Keywords: host defense, inflammasome, macrophages

Introduction

Tuberculosis is caused by *Mycobacterium tuberculosis* and is a serious disease worldwide causing about 2 million deaths each year. The risk of disease is increased by the emergence of acquired immune deficiency syndrome and multidrug-resistant mycobacteria (1). *Mycobacterium tuberculosis* mainly invades and parasitizes macrophages by inhibiting phagosome maturation into phagolysosomes. Macrophages have several recognition systems to defend against mycobacterial invasion. Toll-like receptors (TLRs) recognize mycobacterial components such as glycolipids and CpG motif DNA (2–4). Several recent findings have also indicated that pattern recognition receptors other than TLRs, such as C-type lectin receptors and NOD-like receptors (NLRs), are implicated in the innate recognition of mycobacterial components (5–10). TLRs and C-type lectin receptors are membrane-bound molecules recognizing mycobacterial components in the extracellular compartments, whereas NLRs are present in the cytosol. Thus, several pattern recognition receptors showing distinct subcellular expression patterns recognize structurally and functionally different components of mycobacteria, contributing to protection by evoking an immune response.

Among the NLR family of proteins, NLR pyrin domain containing 3 (NLRP3) is known to activate the inflammasome, a multi-protein platform leading to the processing of the IL-1 family of cytokines (11–14). NLRP3 inflammasome, which is composed of NLRP3, adaptor protein Apoptosis-associated speck-like protein containing a CARD (ASC) and caspase-1, is activated by mycobacteria (15–18). Following activation, inactive caspase-1 is processed by autocleavage via ASC and is converted into the active form of caspase-1 containing

10 kDa/20 kDa subunits. The active form of caspase-1 then cleaves pro-IL-1β and pro-IL-18 into mature forms of IL-1β and IL-18, respectively. The IL-1 family of cytokines, including IL-1β and IL-18, possess potent pro-inflammatory activities (19–21) and are responsible for the host defense against mycobacteria (22–29). However, several studies suggest that NLRP3 or caspase-1, which mediates the processing of the IL-1 family of cytokines, is not essential for the induction of protective immunity to *M. tuberculosis in vivo* (25, 26, 30–32). Thus, the signaling pathway leading to IL-1β/IL-18 production in mycobacterial infection remains controversial.

Recent studies identified that AIM2 (absent in melanoma 2), which possesses HIN-200 and pyrin domains, recognizes cytosolic DNA leading to activation of the inflammasome and secretion of IL-1β and IL-18 (33–36). Several studies have demonstrated that AIM2 is mandatory for the host defense against DNA viruses (Vaccinia virus and mouse cytomegalovirus) and intracellular bacteria (*Francisella tularensis* and *Listeria monocytogenes*) (37–41). However, the role of AIM2-dependent inflammasome activation in mycobacterial infection remains unknown.

In this study, we analyzed the role of AIM2 in mycobacterial infection. AIM2-deficient mice were highly sensitive to *M. tuberculosis* infection. AIM2-deficient macrophages showed impaired activation of the inflammasome and defective production of IL-1β and IL-18 after *M. tuberculosis* infection. Genomic DNA from *M. tuberculosis* was present within the cytosol after infection and induced activation of the inflammasome in an AIM2-dependent manner. These findings demonstrate the critical role of AIM2 in *M. tuberculosis* infection.

Methods

Mice and bacteria

The *Aim2* gene was isolated from genomic DNA extracted from embryonic stem cells (V6.5) by PCR using Elongase Enzyme Mix (Invitrogen). The targeting vector was constructed by replacing a 2.5-kb fragment encoding the exons of *Aim2* with a neomycin-resistance gene cassette and a herpes simplex virus thymidine kinase gene driven by the PGK promoter for negative selection. After transfection of the targeting vector into embryonic stem cells, colonies resistant to both G418 and ganciclovir were selected and screened by PCR and Southern blot. Homologous recombinants were microinjected into blastocysts of C57BL/6 female mice, and heterozygous F1 progenies were intercrossed to obtain AIM2-deficient mice. AIM2-deficient mice and their wild-type littermates from these intercrosses were used and all animal experiments were conducted with the approval of the Animal Research Committee of the Graduate School of Medicine at Osaka University.

Mycobacterium tuberculosis strain H37Rv (ATCC358121) was grown in Middlebrook 7H9-ADC medium for 2 weeks and stored at –80°C until use.

In vivo infection of mice

Mice were intratracheally infected with *M. tuberculosis* H37Rv (1×10^6 CFU per mouse). At 4 weeks after infection, homogenates of the lungs and livers were plated onto 7H10-OADC agar. For histological analysis, the lungs were fixed with 4% PFA, embedded in paraffin, cut into sections, and stained with hematoxylin and eosin or by the Ziehl–Neelsen method.

Harvest of BALF, blood and cells from tissues

Bronchoalveolar lavage fluid (BALF) was collected from uninfected and infected mice by washing the lung airways with phosphate buffered saline (PBS) at 3 weeks post-infection, and blood was collected from the hearts of uninfected and infected mice. $CD4^+$ T cells (4×10^5 cells) were isolated from the spleens at 3 weeks after infection, and then were stimulated with PPD (2 μg ml^{-1}; Japan BCG Laboratory) in the presence of APC (4×10^5 cells) for 48 h.

Mycobacterium tuberculosis genomic DNA extraction

Mycobacterium tuberculosis (1×10^9 CFU) was homogenized with glass beads (0.1 mm; ASONE) and proteins were removed using Phenol/Chloroform/Isoamyl alcohol and Chloroform/Isoamyl alcohol. Genomic DNA was precipitated using isopropanol.

Cell culture and stimulation

Mice were intraperitoneally injected with 4% thioglycollate (Sigma) and 3 days later macrophages were isolated from the peritoneal cavity. Cells were stimulated with LPS (200 ng ml^{-1}) for 3 h and then transfected with poly(dA:dT) (Sigma) or *M. tuberculosis* DNA using Lipofectamine 2000 according to the manufacturer's instructions (Invitrogen). Peritoneal macrophages were infected with *M. tuberculosis* (MOI of 3) for 6 h. Cells were washed three times with PBS and then incubated for 24 h.

ELISA

The concentration of IFN-γ, IL-1β or IL-12p40 in culture supernatants was measured by ELISA according to the manufacturer's instructions (R&D Systems). The ELISA kit for IL-18 was purchased from Medical & Biological Laboratories.

Immuno-precipitation and immuno-blot analysis

Supernatants were precleared with protein G–Sepharose (GE Healthcare), incubated with anti-caspase-1 p10 rabbit antibody (2 μg; Santa Cruz Biotechnology). Cell pellets were lysed in lysis buffer (1% Nonidet P-40, 150 mM NaCl and 50 mM Tris-HCl, pH 7.5) and together with the immuno-precipitants, separated on SDS-PAGE and transferred to PVDF membranes (Millipore). The membranes were incubated with anti-caspase-1 p10 antibody (1:200) and anti-β-actin antibody (1:500; Sigma). Bound antibody was detected with SuperSignal West Dura Extended Duration Substrate (Thermo).

Immuno-fluorescence analysis

Mycobacterium tuberculosis genomic DNA was labeled with Hoechst 33342 (100 ng ml^{-1}; Invitrogen) by incubation for 24 h. Hoechst-labeled *M. tuberculosis* was washed five times with PBS before use. RAW264.7 cells were infected with Hoechst-labeled *M. tuberculosis* (MOI of 3) for 6 h, washed three times with PBS and then incubated for 24 h. Cells were fixed with 4% PFA and permeabilized with 0.4% saponin. The cells were incubated with rabbit anti-Rab7 antibody (1:200; Santa Cruz Biotechnology) or rabbit anti-AIM2 antibody (1:200; Santa Cruz Biotechnology) or rat anti-LAMP1 antibody (1:200; BD Biosciences) for 1 h at room temperature. Cells

were then incubated with Alexa 488 anti-rabbit IgG antibody (Invitrogen) or Alexa 594 anti-rat IgG antibody (Invitrogen) for 40 min at room temperature. The immuno-stained cells were mounted with ProLong Gold antifade reagent (Invitrogen) on glass slides and analyzed using a fluorescence microscope (FV1000-D IX81; Olympus).

Statistical analysis

Differences between control and experimental groups were evaluated using Student's *t* test. Values of $P < 0.05$ were considered to indicate statistical significance.

Results

Aim2$^{-/-}$ mice are highly susceptible to Mycobacterium tuberculosis infection

To assess the *in vivo* role of AIM2, we generated AIM2-deficient mice by gene targeting (Supplementary Figure 1A is available at *International Immunology* Online), which was confirmed by Southern and northern blot analyses (Supplementary Figure 1B and C is available at *International Immunology* Online). *Aim2$^{-/-}$* mice were born at normal Mendelian ratios, developed normally and showed no apparent abnormalities when housed in our specific pathogen-free facility. Several previous studies demonstrated that AIM2 recognizes cytosolic DNA, leading to caspase-1 activation and subsequent processing of the IL-1 family of cytokines, such as IL-1β and IL-18 (33–36, 39). Therefore, we first analyzed the response to synthetic B-form double-stranded DNA [poly(dA:dT)] in *Aim2$^{-/-}$* macrophages. Peritoneal macrophages were collected from wild-type and *Aim2$^{-/-}$* mice and then transfected with poly(dA:dT) into the cytosol after priming with LPS. In immuno-blot analysis, a 10 kDa active form of caspase-1 (p10) was detected in wild-type macrophages stimulated with poly(dA:dT). In contrast, the cleaved p10 form of caspase-1 was not detected in *Aim2$^{-/-}$* macrophages (Supplementary Figure 2A is available at *International Immunology* Online). In addition, poly(dA:dT)-induced secretion of IL-1β and IL-18 into the culture supernatants was markedly decreased in *Aim2$^{-/-}$* macrophages, although ATP-induced secretion of IL-1β was normally observed (Supplementary Figure 2B is available at *International Immunology* Online). Thus, in accordance with previous reports, *Aim2$^{-/-}$* mice showed defective DNA-induced activation of the inflammasome.

We examined the involvement of AIM2 in mycobacterial infection using these *Aim2$^{-/-}$* mice. Wild-type and *Aim2$^{-/-}$* mice were intratracheally infected with the virulent H37Rv strain of *M. tuberculosis* and monitored for their survival (Fig. 1A). All *M. tuberculosis*-infected wild-type mice survived to at least 8 weeks post-infection. In contrast, all *Aim2$^{-/-}$* mice died within 7 weeks of infection with *M. tuberculosis*. We also assessed bacterial burdens in the lungs and livers at 4 weeks post-infection (Fig. 1B). Colony-forming unit titers of *M. tuberculosis* in lungs and livers were higher in *Aim2$^{-/-}$* mice than in wild-type mice. We next performed histological analysis of the lungs of mice at 4 weeks post-infection. Gross appearances of the lungs of wild-type and *Aim2$^{-/-}$* mice were markedly different, and many granulomatous changes were evident in *M. tuberculosis*-infected *Aim2$^{-/-}$* mice (Fig. 2A). Hematoxylin and eosin staining

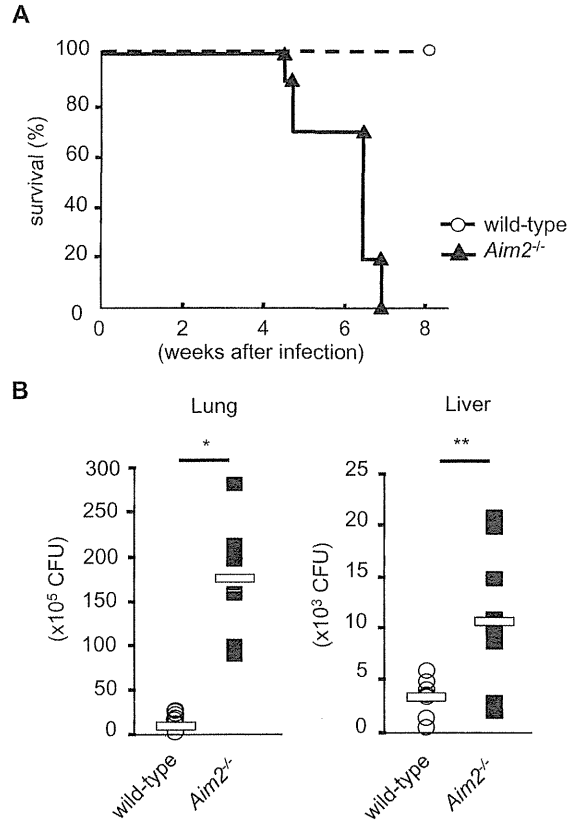

Fig. 1. *Aim2$^{-/-}$* mice are highly sensitive to infection with *M. tuberculosis*. (A) Wild-type ($n = 11$) and *Aim2$^{-/-}$* ($n = 10$) mice were intratracheally infected with *M. tuberculosis* and monitored for their survival. (B) Wild-type ($n = 7$) and *Aim2$^{-/-}$* ($n = 8$) mice were intratracheally infected with *M. tuberculosis*. At 4 weeks after infection, homogenates of the lungs and livers were plated onto 7H10-OADC agar and the CFU titers were counted. Symbols represent individual mice, and bars represent the mean CFU numbers. *, $P < 0.001$; **, $P < 0.01$.

of lung sections from infected *Aim2$^{-/-}$* mice demonstrated infiltration of many inflammatory cells (Fig. 2B). The number of *M. tuberculosis* in the lungs was measured by staining acid-fast bacilli using the Ziehl–Neelsen method (Fig. 2C). In the lungs of *Aim2$^{-/-}$* mice, the number of red-stained *M. tuberculosis* was markedly increased compared with those of wild-type mice. Taken together, these findings demonstrate that *Aim2$^{-/-}$* mice are highly susceptible to intratracheal infection with the virulent H37Rv strain of *M. tuberculosis*.

AIM2 mediates IL-1β/IL-18 production and T_h1 responses in Mycobacterium tuberculosis infection

Recent studies demonstrated that IL-1β is produced from *M. tuberculosis*-infected monocytes and alveolar macrophages mediating the host defense to mycobacteria (22–26, 42). Therefore, we first analyzed the levels of IL-1β in BALF from *M. tuberculosis*-infected mice (Fig. 3A). At 3 weeks after *M. tuberculosis* infection, IL-1β was abundantly detected in BALF from wild-type mice. In contrast, the concentration of IL-1β was profoundly decreased in BALF from *Aim2$^{-/-}$* mice. In addition to IL-1β, IL-18 has also been shown to be important for host resistance to mycobacterial infection (27–29). Therefore, we next

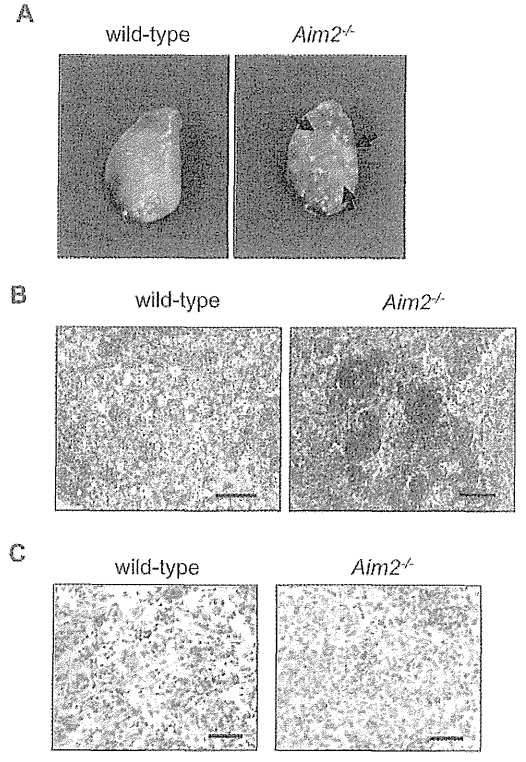

Fig. 2. High susceptibility of *Aim2*$^{-/-}$ mice to infection with *M. tuberculosis*. (A) Lung tissues from wild-type and *Aim2*$^{-/-}$ mice at 4 weeks post-intratracheal infection with *M. tuberculosis*. Arrows are shown to granulomatous lesion. (B) Lung tissue sections were stained with hematoxylin and eosin. Scale bars represent 100 μm. (C) Lung tissue sections were stained by the Ziehl–Neelsen method. Scale bars represent 40 μm.

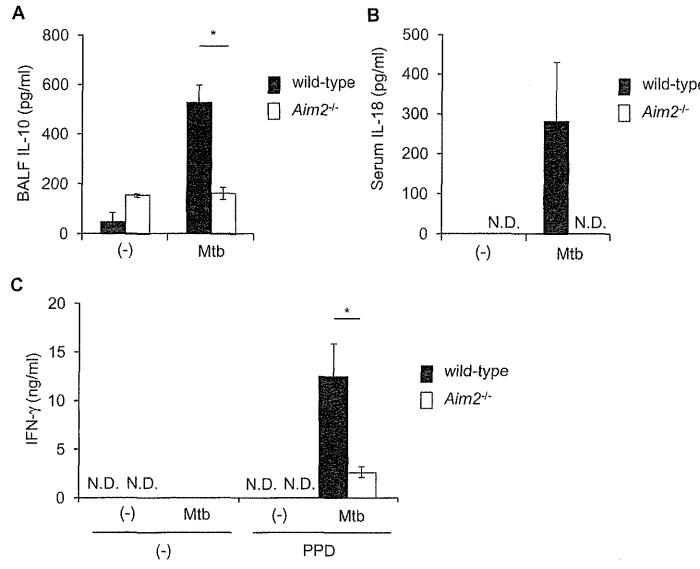

Fig. 3. Impaired production of IL-1β and IL-18 in *M. tuberculosis*-infected *Aim2*$^{-/-}$ mice. (A) BALF was collected from uninfected and infected mice at 3 weeks post-mycobacterial infection. BALF concentration of IL-1β was measured by ELISA. Data are presented as means ± SD of triplicate determinants and are one representative of two independent experiments. *, $P < 0.01$. (B) At 3 weeks after mycobacterial infection, sera were collected from uninfected and infected mice. Concentration of IL-18 was measured by ELISA. Data are presented as means ± SD of triplicate determinants and are one representative of two independent experiments. N.D., not detected. (C) CD4$^+$ T cells were isolated from the spleens of *M. tuberculosis*-uninfected and infected mice. The cells were co-cultured with APC for 48 h in the presence of PPD. The levels of IFN-γ in the cell supernatants were measured by ELISA. Data are presented as means ± SD of triplicate determinants and are one representative of two independent experiments. *, $P < 0.05$. N.D., not detected.

measured the serum levels of IL-18 in *M. tuberculosis*-infected mice (Fig. 3B). Serum concentration of IL-18 was increased in wild-type mice at 3 weeks post-infection. In contrast, IL-18 was not detected in sera from *M. tuberculosis*-infected *Aim2*$^{-/-}$ mice. We also assessed antigen-specific T_h1 responses following infection. CD4$^+$ T cells were isolated from the spleens of wild-type and *Aim2*$^{-/-}$ mice at 4 weeks post-infection and stimulated with a mycobacterial-specific antigen [purified protein derivative (PPD) of *Mycobacterium bovis*] in the presence of antigen-presenting cells (Fig. 3C). PPD stimulation induced marked production of IFN-γ in *M. tuberculosis*-infected wild-type mice. Antigen-specific production of IFN-γ was severely reduced in CD4$^+$ T cells derived from *M. tuberculosis*-infected *Aim2*$^{-/-}$ mice. These results indicate that the absence of AIM2 results in impaired production of IL-1β and IL-18 as well as T_h1 responses after *M. tuberculosis* infection.

AIM2 mediates Mycobacterium tuberculosis-induced inflammasome activation

We assessed the activation of caspase-1 to determine how AIM2-dependent immune responses develop following *M. tuberculosis* infection (Fig. 4A). Cleaved p10 form of caspase-1 was detected in *M. tuberculosis*-infected macrophages of wild-type mice. In contrast, cleavage of caspase-1 was severely reduced in *M. tuberculosis*-infected *Aim2*$^{-/-}$ macrophages.

We also analyzed cytokine production in *M. tuberculosis*-infected macrophages. Peritoneal macrophages from wild-type and *Aim2*$^{-/-}$ mice were infected with *M. tuberculosis* and the levels of cytokines in culture supernatants were measured by ELISA (Fig. 4B). *M. tuberculosis*-induced production of IL-12p40 or IFN-γ was comparable between wild-type and *Aim2*$^{-/-}$ macrophages. However, the production of IL-1β and IL-18 was severely reduced in *Aim2*$^{-/-}$ macrophages. Similar mRNA expression levels of *Il1b* and *Il18* in *M. tuberculosis*-infected wild-type and *Aim2*$^{-/-}$ macrophages were detected using real-time quantitative RT-PCR (Supplementary Figure 3 is available at *International Immunology* Online), indicating that AIM2 controls the production of IL-1β and IL-18 at the post-transcriptional level. Induction of *Ifnb*, encoding IFN-β, was enhanced in *M. tuberculosis*-infected *Aim2*$^{-/-}$ macrophages, confirming previous results (37). Thus, *M. tuberculosis*-infected *Aim2*$^{-/-}$ macrophages show defective caspase-1 activation leading to selective impairment in IL-1β and IL-18 secretion.

Mycobacterium tuberculosis genomic DNA activates AIM2 inflammasome

AIM2 has been shown to recognize cytosolic DNA (33–41). Therefore, we tested whether genomic DNA purified from

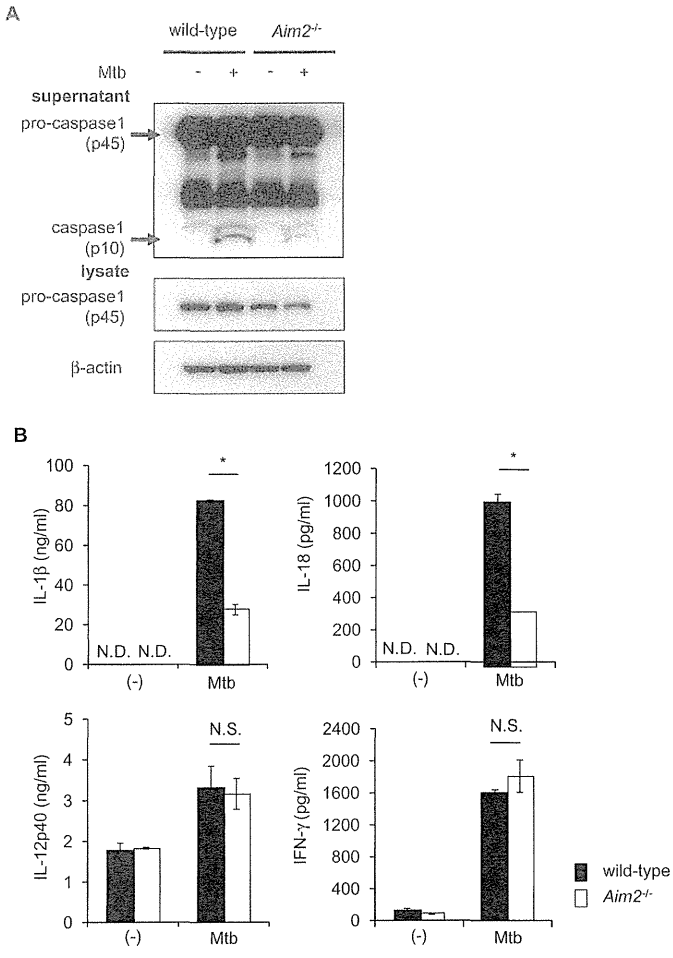

Fig. 4. AIM2-dependent inflammasome activation in *M. tuberculosis* infection. (A) *M. tuberculosis*-infected peritoneal macrophage culture supernatants were immuno-precipitated and the cell pellets were lysed. Caspase-1 specific bands were detected by western blotting and β-actin was used as a control for the cell lysate. One representative of three independent experiments is shown. (B) Thioglycollate-induced peritoneal macrophages were infected with *M. tuberculosis* (MOI of 3). The levels of the indicated cytokines in the culture supernatants were measured by ELISA. Data are presented as means ± SD of triplicate determinants and are one representative of three independent experiments. *, $P < 0.01$. N.S., not significant; N.D., not detected.

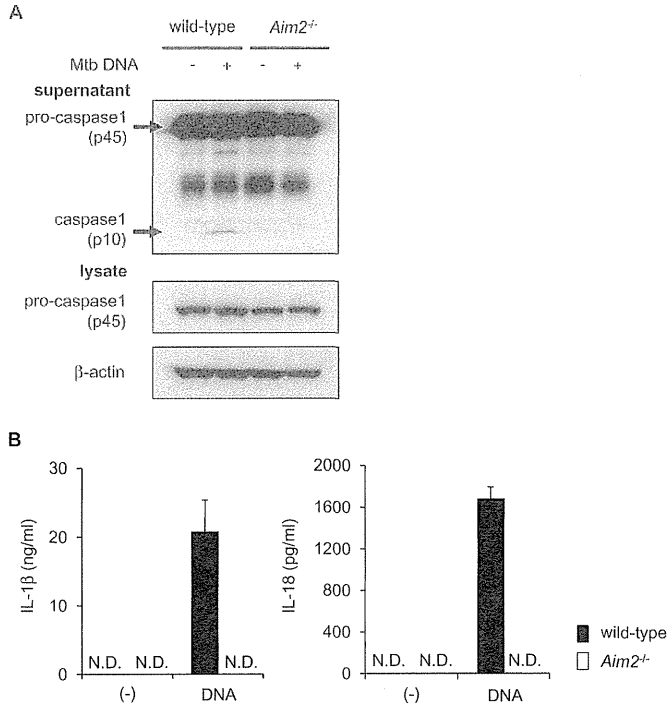

Fig. 5. AIM2 inflammasome is activated by *M. tuberculosis* genomic DNA. (A) Peritoneal macrophages were stimulated with LPS and transfected with Mtb DNA using Lipofectamine 2000. The culture supernatants were immuno-precipitated and the cells were lysed. Caspase-1 specific bands were detected by western blotting. β-actin was used as a control for the cell lysate. One representative of three independent experiments is shown. (B) Thioglycollate-elicited peritoneal macrophages were stimulated with LPS and transfected with Mtb DNA using Lipofectamine 2000. The production of IL-1β and IL-18 in the culture supernatants was measured by ELISA. Data are presented as means ± SD of triplicate determinants and are one representative of three independent experiments. N.D., not detected.

M. tuberculosis (Mtb DNA) activates caspase-1. Mtb DNA was transfected into the cytoplasm of peritoneal macrophages primed with LPS and analyzed for caspase-1 activation (Fig. 5A). The cleaved p10 form of caspase-1 was detected in LPS/Mtb DNA-stimulated wild-type macrophages. In contrast, the active form of caspase-1 was not induced in *Aim2*$^{-/-}$ macrophages stimulated with LPS/Mtb DNA. We also analyzed the secretion of IL-1β and IL-18 (Fig. 5B). Wild-type peritoneal macrophages stimulated with LPS/Mtb DNA secreted substantial amounts of IL-1β and IL-18. In contrast, the production of IL-1β and IL-18 was profoundly reduced in *Aim2*$^{-/-}$ macrophages. These findings indicate that AIM2 mediates Mtb DNA-dependent induction of caspase-1 activation and subsequent IL-1β/IL-18 secretion.

Mycobacterium tuberculosis genomic DNA is co-localized with cytosolic AIM2

We next determined the cellular compartment where Mtb DNA is recognized by AIM2. Recent studies demonstrated that virulent *M. tuberculosis* escapes from phagosomes into the cytosol (43). *Mycobacterium tuberculosis* was incubated with Hoechst 33342 to label genomic DNA and then infected into RAW264.7 macrophages. Some Mtb DNA was not co-localized with Rab7, which is recruited to the phagosomal membrane (Fig. 6A). Although LAMP1 is enriched in the phagolysosomal compartment, some Mtb DNA was not co-localized with it (Fig. 6B, upper panels). In contrast, genomic DNA from non-virulent *M. bovis* bacillus Calmette-Guerin (BCG) was fully merged with phagosome markers, Rab7 and LAMP1 (Supplementary Figure 4 is available at *International Immunology* Online). These findings indicate that Mtb DNA is present in the cytosol. We further visualized cytosolic AIM2 (Fig. 6B, lower panels). Mtb DNA, which was not present within the phagosome, co-localized with AIM2. We also analyzed co-localization of AIM2 and Mtb DNA in peritoneal macrophages (Supplementary Figure 5 is available at *International Immunology* Online). As was the case in RAW264.7 macrophages, Mtb DNA was merged with